When a mudstone was actually a "sand": Results of a sedimentological investigation of the bituminous marl formation (Oligocene), Eastern Carpathians of Romania

Juergen Schieber [a], Crina Miclăuş [b, c] ✉, Anca Seserman [b], Bei Liu [a], Juan Teng [a]

[a] Department of Geological Sciences, Indiana University, Bloomington, Indiana, USA
[b] Department of Geology, Alexandru Ioan Cuza University, 20A Carol I Blvd, 700505-Iaşi, Romania
[c] Doctoral School of Geosciences, Alexandru Ioan Cuza University, Iaşi, Romania

The text below is exactly the same text as published in Sedimentary Geology (Sedimentary Geology, v. 384, p. 12-28), but has been augmented with additional figures. These additional figures ("cut" from the original manuscript) have consecutive letter designations in the form "[extra Figure A]" etc., and are further differentiated through the use of italics for the figure captions.

Abstract

   The bituminous marl formation (BMF) is an important source rock in Romania. At the study location, in the Eastern Carpathians, the BMF composition is dominated by calcite (coccolith debris, cement) and diagenetic silica, with the remainder consisting largely of detrital clays, quartz and minor feldspar. Abundant intervals with soft sediment deformation, likely slump deposits, alternate with thinly layered marls that may locally contain layers and lenses of rippled and cross-laminated sandstone. The latter suggest intermittent action of traction currents. Although the fine grained nature and abundant nanoplankton content of the marls suggest that they originated via pelagic settling through the water column, upon close inspection, they consist of flattened sand-size yet fine-grained aggregates (soft clasts). Experimental studies suggest that these were likely eroded from the seabed and transported in bedload by bottom currents. Inclined fabric elements within marls suggest that soft clasts formed ripples, and that marl layers are the depositional consequence of ripple migration. Whereas typical marl layers probably reflect migration of small ripples of a few cm's height, there are also cross-bedded marly beforms with ca. 20 cm pre-compaction relief that by size are muddy megaripples. Unlike in sand, where bedform hierarchy reflects increasing flow velocity, muddy megaripples more likely are a reflection of bottom current systems of substantial duration.
With marl layers as well as interbedded sands recording bottom current activity, the BMF represents a combination of slope processes and bottom current activity. The likely environment of deposition is a lower slope to basin setting with contour currents reworking pelagic sedimentation and intermittent sediment supply by slumping.

Keywords: mud, marl, lenticular fabric, mud megaripple, bottom current, mud reworking

1. Introduction and Geological Setting

   The bituminous marl formation (BMF) belongs to the sedimentary succession of the Moldavidian Basin (Săndulescu, 1988), a remnant of one of the Alpine Tethys branches which evolved inside of the so-called Carpathian Embayment (sensu Balla, 1986) after Cretaceous tectonism. The basin fill consist of Cretaceous-Miocene deposits (Micu and Gheța, 1986; Grasu et al., 1988; Ștefănescu, 1995; Mutihac, 1992; Mărunțeanu, 1999; Melinte et al., 2002; Melinte-Dobrinescu et al., 2008; Belayouni et al., 2009; Guerrera et al., 2012) that were folded and thrusted to form several nappes (Teleajen, Macla, Audia, Tarcău, Vrancea, and Pericarpathian from internal to external position; Fig. 1) during the Miocene (Săndulescu, 1988; Roure et al., 1993; Ellouz and Roca, 1994; Mațenco, 2017). The Moldavidian Basin was a foreland basin system (DeCelles and Giles, 1996) with the foredeep migrating from the Teleajen Nappe sedimentation area in the Cretaceous to the Tarcău Nappe internal sedimentation area during the Paleogene and finally to the Pericarpathian Nappe area in the Miocene (Grasu et al., 1999; Guerrera et al., 2012).
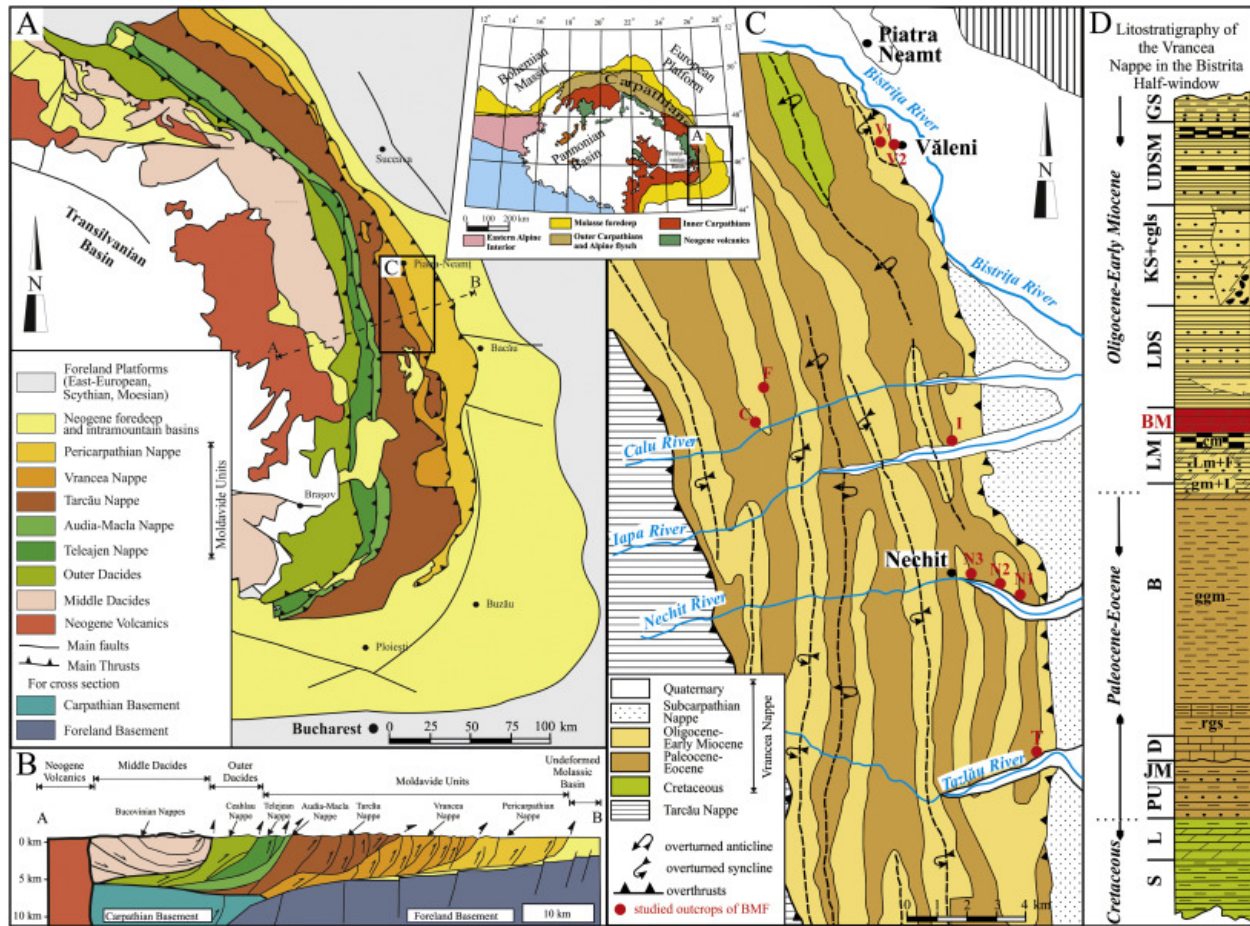
Figure 1: A. Geology of the Eastern Carpathians and structural cross section (not at scale) sketch (B) showing the main thrust sheets (based on Săndulescu and Dumitrescu, 1970). The studied area is indicated by the black rectangle; C. The study area in Eastern Carpathians (Romania), with sample localities marked in red, as well as a summary stratigraphic column (D) with the BMF marked in red (based on Micu, 1976; Grasu et al., 1988), T marks Tazlău section (see Fig. 2). Key: S – Sărata Formation; L – Lepşa Formation; PU – Piatra Uscată Formation; JM – Jgheabu Mare Formation; D – Doamna Limestone Formation; B – Bisericani Formation (rgs – red and green shale; greenish-grey mudstone; gm+L – Globigerina marls and Lucăceşti Sst); LM – lower menilite formation (Lm+F - Linguresţi Marls and Ferăstrău Sst; cm – compact menilites); BM – bituminous marls formation; LSM – lower dysodilic shale formation; KS+cgls – Kliwa Sst and conglomerates; UDSM – upper dysodilic shale and menilites formation; GS – Gura Soimului Formation.

    The study area is located in one of the outermost nappes of the Eastern Carpathians, the Vrancea Nappe (Fig. 1), where the BMF reaches its maximum thickness of about 70 m. The Oligocene-Miocene sedimentary succession of the Vrancea Nappe was deposited on the internal flank of a prominent forebulge that also functioned as a source area that supplied coarse clastics, such as quartzose sands and gravels with greenchist clasts (Miclăuş et al., 2009).

    Whereas in early studies (prior to 1950) organic-rich Oligocene units were thought to have

been deposited in nearshore environments or in shallow marine lagoons and even brackish water (e.g. Athanasiu et al., 1927; Filipescu, 1934), perspectives changed once turbidites became an accepted model for deep water clastic deposition. For example, Anastasiu et al. (1994, 1995) now consider that the strata of the outer "flysch" zone, of which the Vrancea Nappe is part, were deposited in a deep water continental margin to abyssal plain setting. A deep water, euxinic environment, dominated by settling was envisioned by Săndulescu and Micu (1989), and under consideration of all paleontological information, Bădescu (2005) suggested that a water depth of 400-600 m value would be appropriate.

This study is the outcome of detailed sedimentologic and petrographic studies of the BMF in the vicinity of Piatra Neamț, Romania (Fig. 1). Key insights are that the marls contain abundant sand-size fine grained composite particles that represent soft mud rip-ups, and that these were eroded by bottom currents from the contemporaneous seabed, transported in bedload, and compressed into thin lenses in the course of compaction. In essence, the marl layers are "unconventional" sand deposits. As such, the study adds to a growing body of work that shows that mudstones, which once were thought to represent low energy depositional conditions, may actually record substantial current and/or wave activity in spite of their apparently fine grain size (Schieber et al., 2007a; Plint et al., 2012; Könitzer et al., 2014; Laycock et al., 2017; Newport et al., 2018; Li and Schieber, 2019). Our observations suggest that deposition of the BMF marls was strongly dominated by current flow, and that the likely environment of deposition was a lower slope to basin setting where contour currents reworked pelagic deposits and intermittent sediment supply provided by slumping.

2. Methods

Outcrops were described and sampled during two field visits in 2013 and 2016. More than 100 samples were collected and slabbed for detailed examination of macroscopic sedimentary features. For a subset of samples, 46 polished thin sections were prepared for examination with a petrographic microscope (Zeiss Photo III). Areas of specific interest identified by petrographic microscope were then studied at higher magnification by scanning electron microscope (SEM; FEI Quanta 400), in an effort to image microfabrics, grain relationships, and diagenetic features. For some samples, argon ion-milled surfaces were prepared to study textural features in highest detail by SEM (Schieber, 2013; Mastalerz and Schieber, 2017).

Major and trace elements were measured on 16 slabbed samples by portable x-ray fluorescence (pXRF; Rowe et al., 2012) such that the 11 mm diameter analysis spot was centered on single laminae in order to capture the range of lamina by lamina compositional variability. As many as 11 layer analyses were performed on a given sample, and a total of 110 analyses were acquired with a pXRF analyzer (Thermo Niton XL3t).

3. Observations

3.1. General Appearance

In the study area, the BMF is a hard and erosion resistant interval that forms rapids in river valleys and affords excellent exposures that show sedimentary features in fine detail [*extra Figure A*]. In between such river-polished outcrops, however, exposures are discontinuous and exposure quality is comparatively poor.

Figure A: outcrop of the BMF at Tazlău, in a clean washed river exposure. Visible layering is at the cm-scale.

On freshly cut surfaces the BMF shows various shades of brownish coloration, on account of its inherent bitumen content. During outcrop weathering, the bitumen component is oxidized and leaves behind thin and typically parallel layers of gray to beige mudstone, ranging in thickness from less than a mm to 1 cm or more. The layering is a result of alternating marl layers with different composition (variable carbonate and quartz content) and interspersed layers of sandstone. The mudstone contains abundant calcite in the form of fossil debris and cements, in addition to clays and quartz silt, and thus fits the definition of a marl (Pettijohn, 1957), a usage that we will adhere to for this study.

In addition to thinly layered gray marls, other characteristic features of the BMF in the study area are abundant intervals that show soft sediment deformation of variable intensity and sandy layers of variable thickness (Fig. 2). These disturbed intervals may measure from a few dm's to several meters in thickness and range from layers dominated by convolute bedding (Fig. 3A), to convolute beds with intact blocks of undeformed sediment (Fig. 3B), to intervals that internally show coherent bedding but have sheared contacts to underlying strata (Fig. 3C). Deformation can also result in various degrees of mixing and homogenization of marly and sandy layers and show coherent marl fragments within a mixed matrix of sand and marl (Fig. 3D&F). Associated with above described features one can also find intervals with slightly disturbed layering (Fig. 3E).
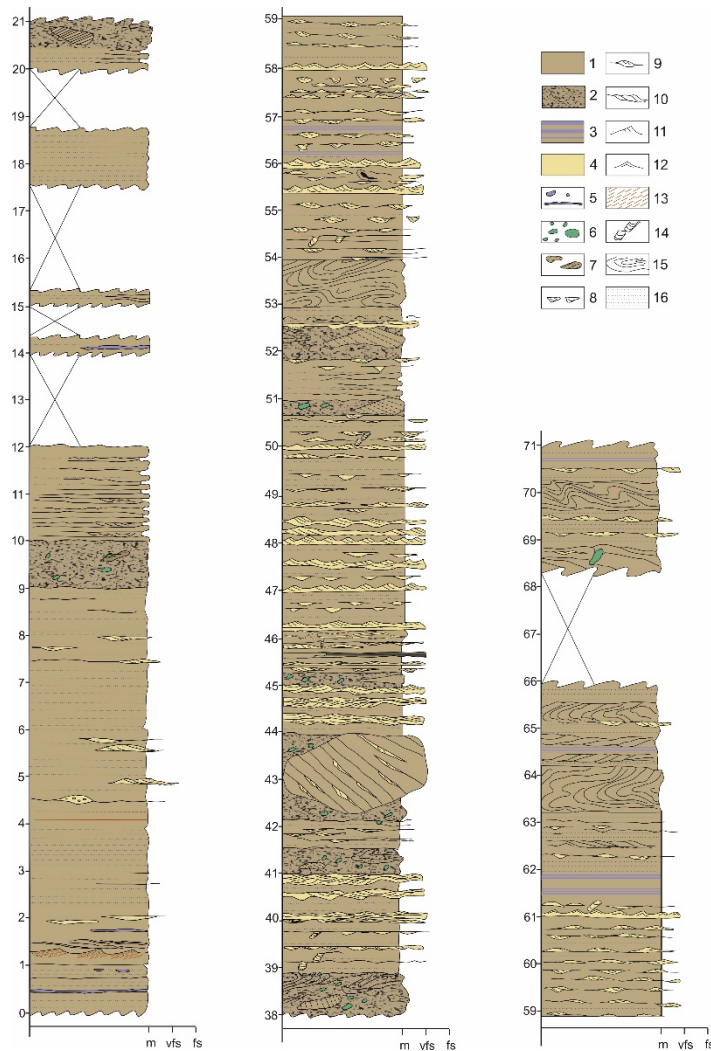
Figure 2: Lithologic log of BMF at the Tazlău River (point T on Fig. 1C). Key: 1 - bituminous marls; 2 - unstructured marls (matrix of paraconglomerate); 3 - silicified marl beds; 4 - sandstones; 5 - siliceous nodules/beds; 6 - greenschist clasts (pebble to boulder size); 7 - bituminous marls clasts (boulders to block size); 8 - ball and pillow structures; 9 - lenticular sand beds; 10 - set of cross-bedded marl; 11 - current ripples; 12 - symmetric ripples; 13 - imbricated fish scales; 14 - sediment filled fissures; 15 - slumps and/or convolute bedding; 16 - bounding surfaces of marl layers with carbonatic and/or terrigenous sand laminae.

Figure 3 (next page): Soft sediment deformation features. (A) A marl bed with convolute bedding and sharp lower and upper boundaries interbedded with undisturbed BMF. (B) A bed similar to (A) but with large block of comparatively undeformed sediment. (C) Two bodies of sediment in unconformable contact (red arrows). The layers of the upper and the lower block are truncated at the contact, interpreted as a slump related shear plane. (D) Examples of sediment mixing in the interior of a deformed deposit. Near the top a sand layer that has incorporated variably deformed chunks of marl (turquoise arrows). In the center we see a layer where sand and marly matrix are pretty well blended together. Yellow arrows point to pieces of still coherent marl, and green arrows point to greenish clasts of metamorphic origin. (E) An interval of even but slightly disturbed layering. Yellow arrows point to small scale faults that suggest stretching of partially lithified sediment. (F) A closer view of the deformed fabric as seen in (B) and the lower third of (D). There are pieces of sheared sediment that still show preserved internal layering (e.g. that marked by yellow arrows), and other regions where the primary fabric has been lost and we see a finely mixed matrix (e.g. turquoise arrows).
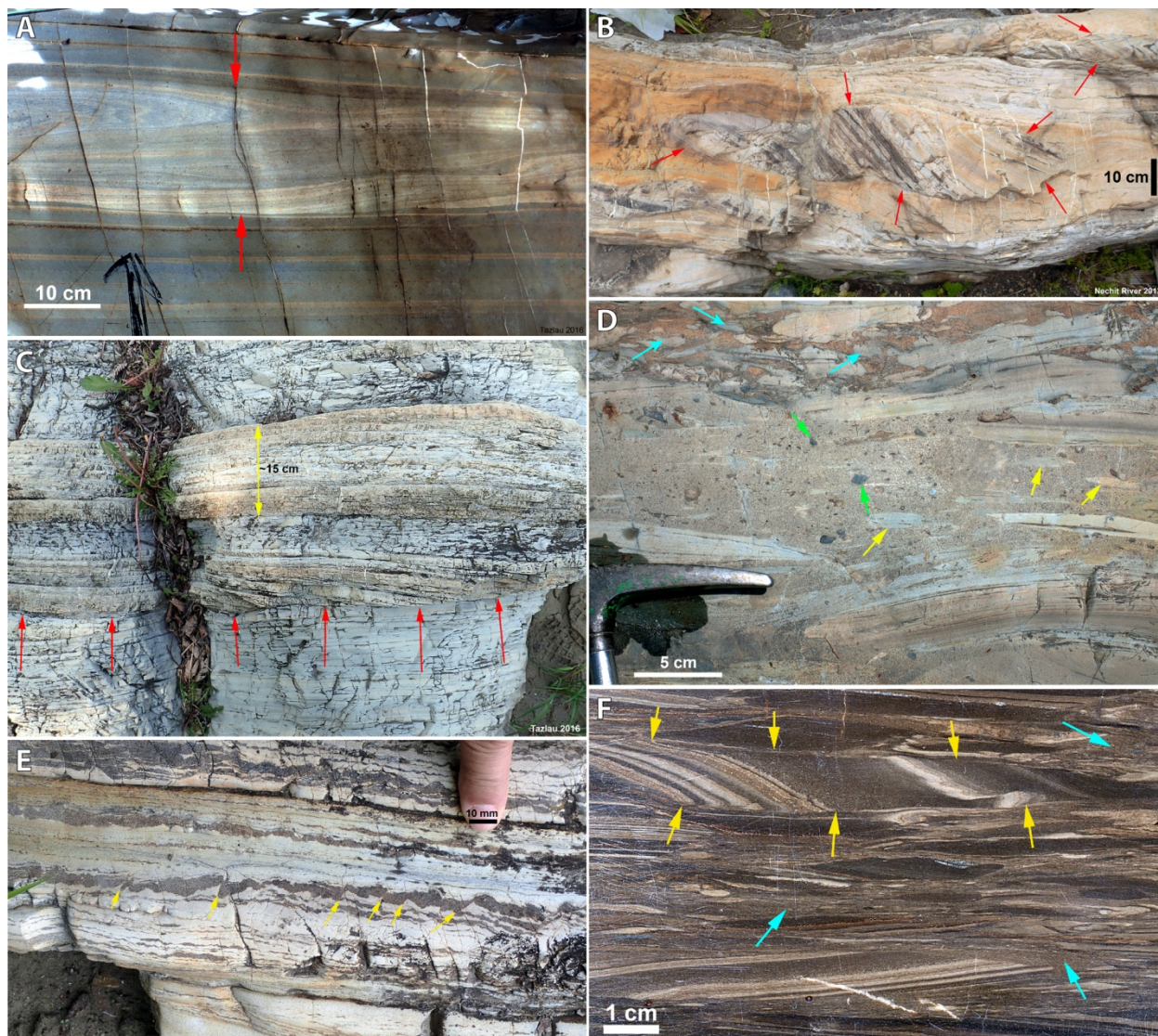
Figure 3: see caption on previous page.

In places one also finds vertical sand fills and clastic dikes with prominent display of differential compaction around these features [*extra Figure B*]. These sand bodies appear tabular and not of erosional nature.

Sandy layers range from as thin as a mm to as much as 20 cm in thickness and show sharp lower and upper contacts, basal load structures and scouring, as well as internal cross-lamination and rippled upper surfaces [*extra Figure C*]. Internal cross-lamination can be complex in its spatial arrangement, with internal discontinuities separating successive cross-laminated portions. Changing dip directions between intervals suggest interval to interval shifts in flow direction.

Figure B: A fissure filled with sand and green pebbles (metamorphic, green arrows). The infilling sediment is not of the same composition than that of the sand layer that drapes over the top (yellow arrow). Differential compaction for sediment horizons marked by arrows a-b and a'-b' suggests that the sediment contained about 60 vol % water when the fissure was filled.

Sandy layers range from as thin as a mm to as much as 20 cm in thickness and show sharp lower and upper contacts, basal load structures and scouring, as well as internal cross-lamination and rippled upper surfaces [*extra Figure C*]. Internal cross-lamination can be complex in its spatial arrangement, with internal discontinuities separating successive cross-laminated portions. Changing dip directions between intervals suggest interval to interval shifts in flow direction.
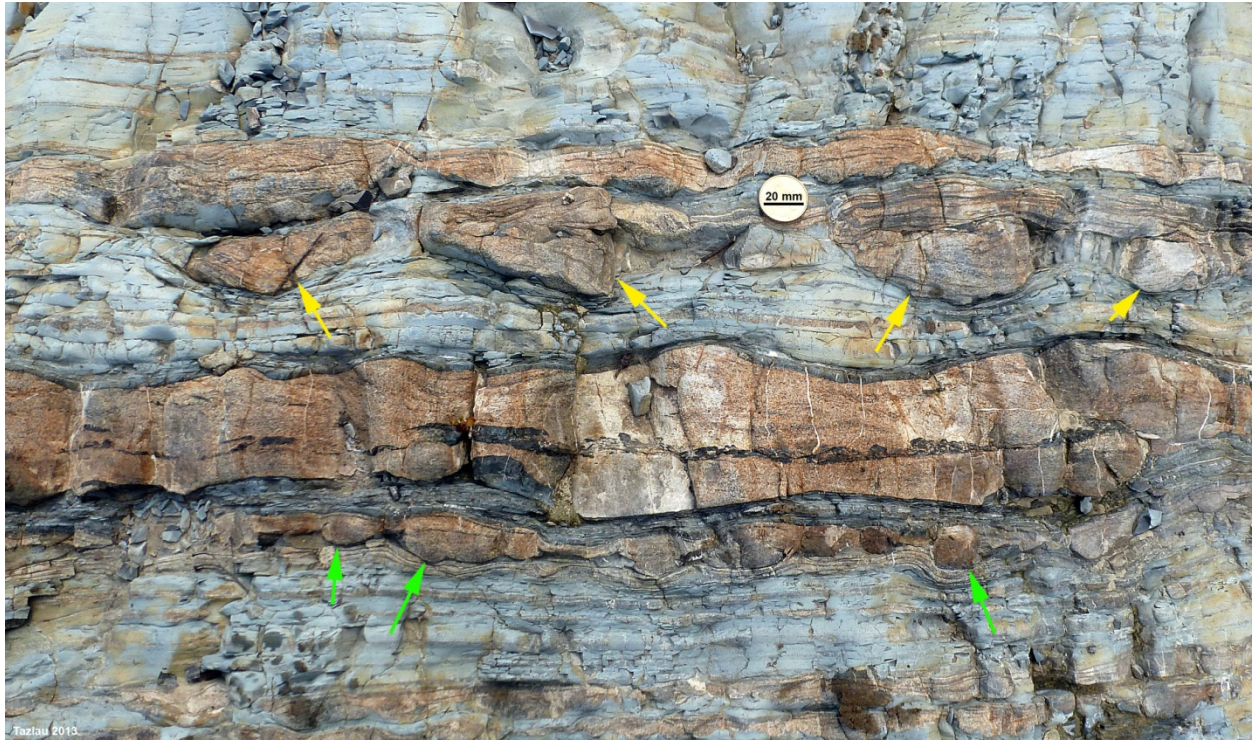
Figure C: Interbeds of sandstone (brownish) separated by marl-dominated intervals. Well developed ball and pillow structures (yellow arrows) and load casts at the base of sandstone beds (green arrows). Not much evidence of basal scouring and erosion in this image.

Whereas the load structures suggest a water-rich soft substrate that these sand ripples were migrating across, the apparent sediment load capacity (sediment stiffness) appears to vary over short vertical distances (Fig. 4). For example, in Figure 4, intervals marked with red double arrows show marl laminae with thin sand lenses that lack basal load casts, whereas intervening intervals have thicker marl laminae (5-10 mm) and also have thickened sand lenses with basal load structures, suggesting possibly low sedimentation rates and better sediment dewatering for the red arrow marked intervals.
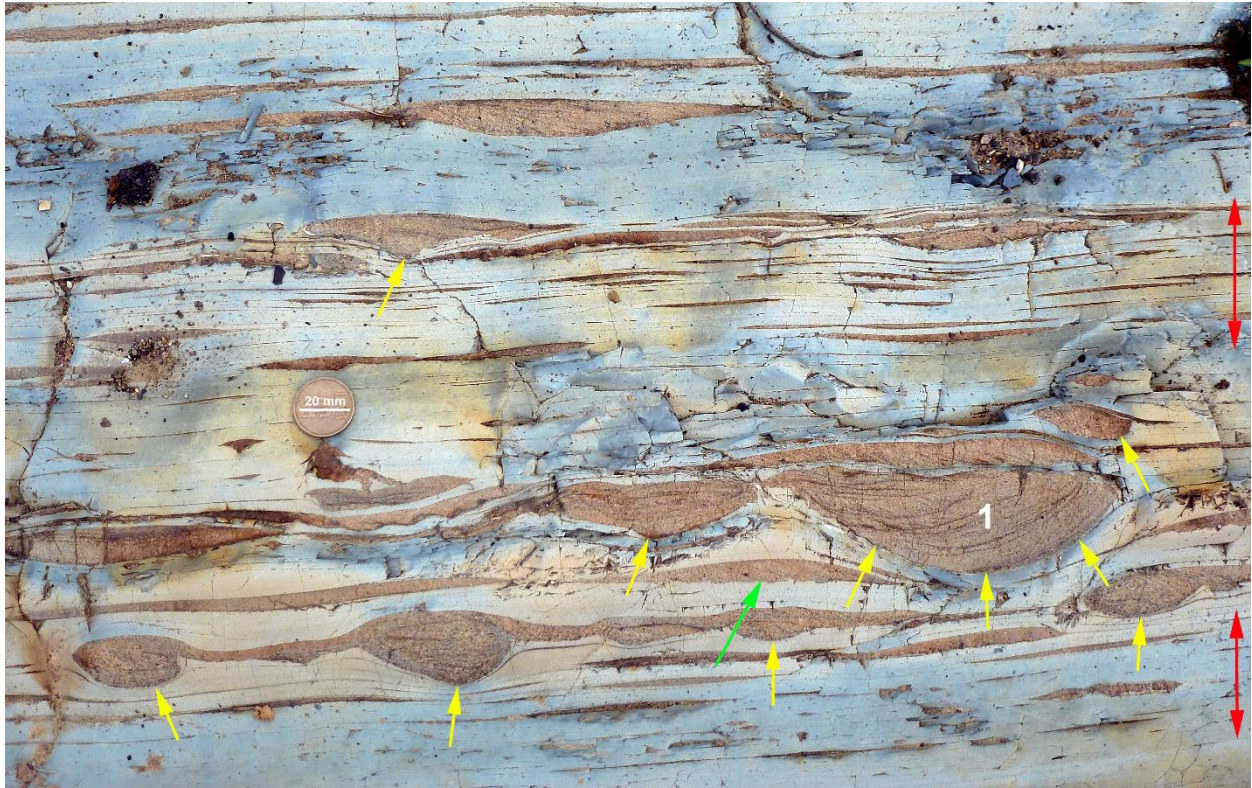
Figure 4: Multiple ripples, some are "loadcasted" (Dzulynski and Kotlarczyk, 1962) because they migrated across a soft water-rich substrate (yellow arrows), whereas others do not show a sunken base and seem to have migrated over a firmer substrate (green arrow, intervals marked by red double arrows). Differential compaction associated with ripple marked "1" suggests a sediment water content of about 85 vol %.

Petrographically, these sandstone layers and lenses are dominated by quartz grains, with minor amounts of feldspar, metamorphic rock fragments, glauconite pellets, and fossil debris. The space between sand grains is occupied with either calcite spar cement or with a fine grained matrix that is indistinguishable from the material that composes the marl layers (Fig. 5). The marl component can show deformation around sand grains and squeezing into pore spaces, strongly suggesting that the marl matrix consists of soft, water-rich rip up clasts of fine grained surface sediment. The relative proportions of all these components can be highly variable from layer to layer.
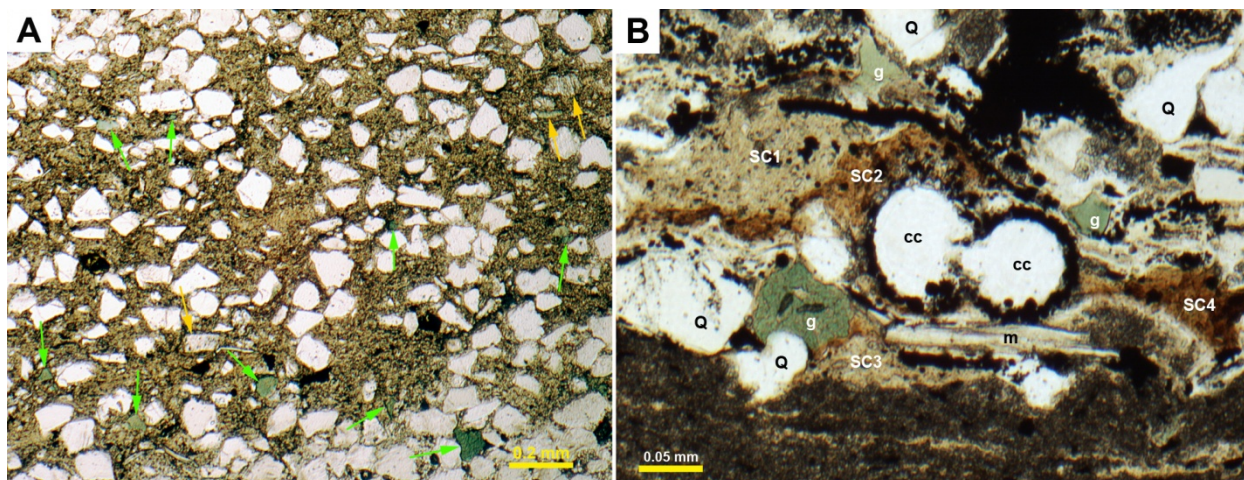
Figure 5: (A) Photomicrograph from a sand bed like seen in Figure 4. Green arrows point to glauconite pellets, orange arrows point to feldspar grains and metamorphic rock fragments. Most of the clear grains are quartz. Note abundant fine grained matrix between quartz grains. (B) Detail view of another sand layer. Q=quartz; g=glauconite; m=mica; cc=chalcedony fill of foram test. The fine "matrix" between other grains has the appearance of deformed fine grained aggregates (SC=soft clast) of sand size. There are two different types of soft clasts. SC1/3 looks like it was derived from the underlying marl bed, but the more brownish SC2/4 is probably more carbonaceous and was brought from elsewhere.

When examined in more detail, the marly intervals of the BMF can be shown to be a three component system, consisting of interstratified strongly calcitic layers (1), marly layers (2), and sandy layers (3). Using these components one can distinguish 1) bituminous marl with calcareous laminae, 2) bituminous marl with thin sandy laminae and minor calcareous laminae, and 3) bituminous marl with thin sandy lenses (Fig. 6).

Whereas the proportional abundance of these layer types could in principle be used to define for example three lithofacies types, such as illustrated in Figures 6 and 7, when looked at closely one realizes that there is a compositional continuum rather than distinct groupings. Given the presumed pelagic to hemipelagic setting of the BMF, continuous mixing of pelagic (biogenic calcite) and terrigenous inputs (clays) appears a feasible model.
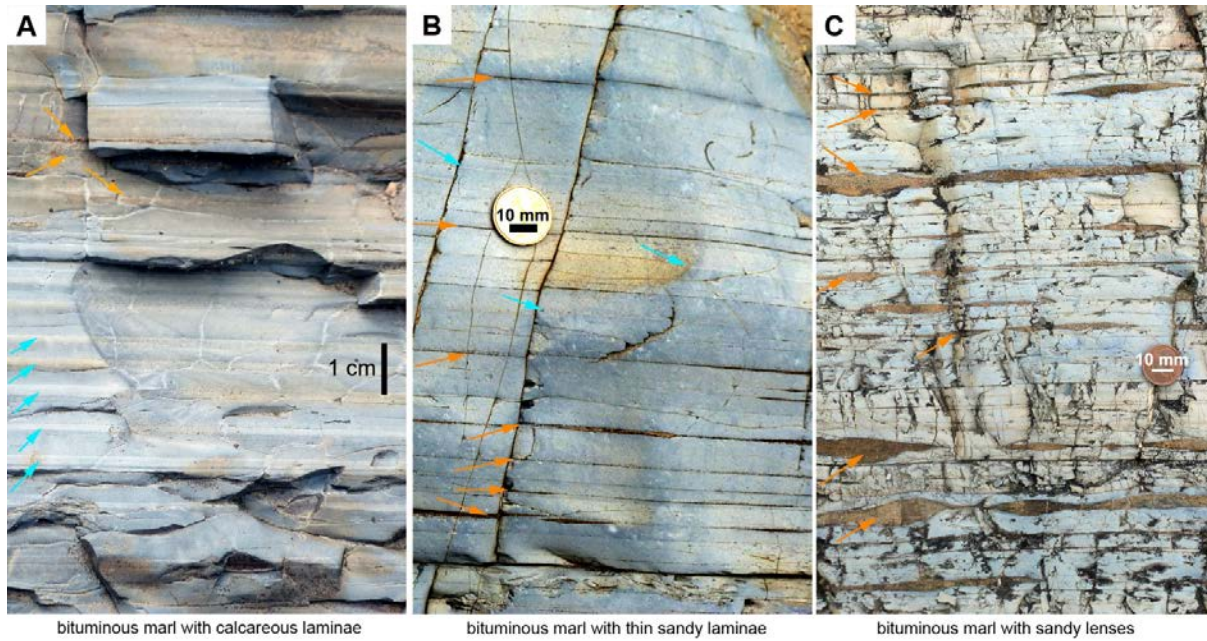
bituminous marl with calcareous laminae   bituminous marl with thin sandy laminae   bituminous marl with sandy lenses

Figure 6: Three views of the BMF, calcite-rich at left (A), calcareous and sandy in the middle (B), and sand-rich at right (C). Orange arrows point to sand layers, blue arrows point to carbonate-rich layers. The visible layers measure in the mm to cm range, although in detail mm-scale layering dominates (Fig. 7).
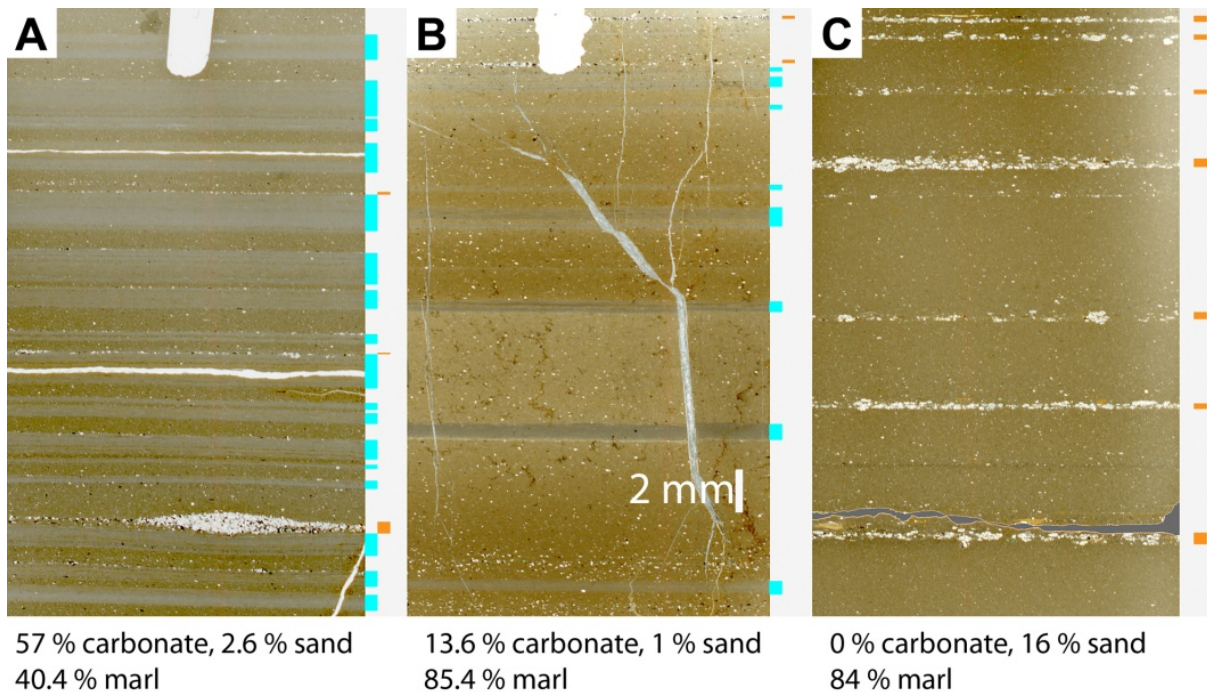

57 % carbonate, 2.6 % sand
40.4 % marl

13.6 % carbonate, 1 % sand
85.4 % marl

0 % carbonate, 16 % sand
84 % marl

Figure 7: A set of thin section scans (all at same scale) that more closely illustrates the association of layers as seen in outcrop (Fig. 6). Calcite-rich layers are marked in blue at the right margin of each thin section, and sandy layers are marked in orange. The unmarked remainder represents layers of generic marl. At left (A) calcite-rich layers are abundant, at right (C) sandy layers are common, and in the middle (B) both calcareous and sandy layers are present.

12

3.2. Petrographic Composition

SEM examination of polished thin sections and ion milled surfaces (Fig. 8) shows the main ingredients of the BMF marl layers illustrated in Figure 7. The matrix of the marl layers consists of a mixture of clays, calcareous microfossil debris (dominantly coccoliths and minor foraminifera), organic matter/kerogen, and early diagenetic cements of calcite and quartz. Within this matrix we may also find scattered phosphatic debris (fish scales, bones) and sand grains (quartz, feldspar, glauconite). Calcite-rich layers consist almost exclusively of coccolith debris and pelagic (coccolith) fecal pellets, and sandy layers are dominated by sand size grains of quartz and minor feldspar. In places, fine grained aggregates/lenses consist of a mixture of carbonate debris and pyrite that has replaced finely textured diatom fragments [*extra Figure D*].

Figure 8 (see below, following page): Key petrographic features of marl beds as seen by SEM. (A) Typical marl matrix with some shell fragments (calcite). (B) Closer view of matrix with clay-rich streaks (yellow arrows) mingled with calcareous matter, diagenetic quartz, and kerogen streaks (white arrows). (C) Detail view of matrix with dark kerogen streaks (white arrows), detrital quartz (Q), diagenetic quartz (q), and coccolith debris (c). (D) Spatial relationships between clay-rich domains (yellow arrows), carbonate cement (medium gray, smooth), coccolith debris (c, light gray), and small clusters of diagenetic quartz grains (q). (E) Low magnification view of scattered detrital quartz sand grains (Q) within marly matrix. (F) Typical view of calcite-rich layer, with abundant coccolith debris, some preserved coccolithospheres (arrows) and calcite cement.
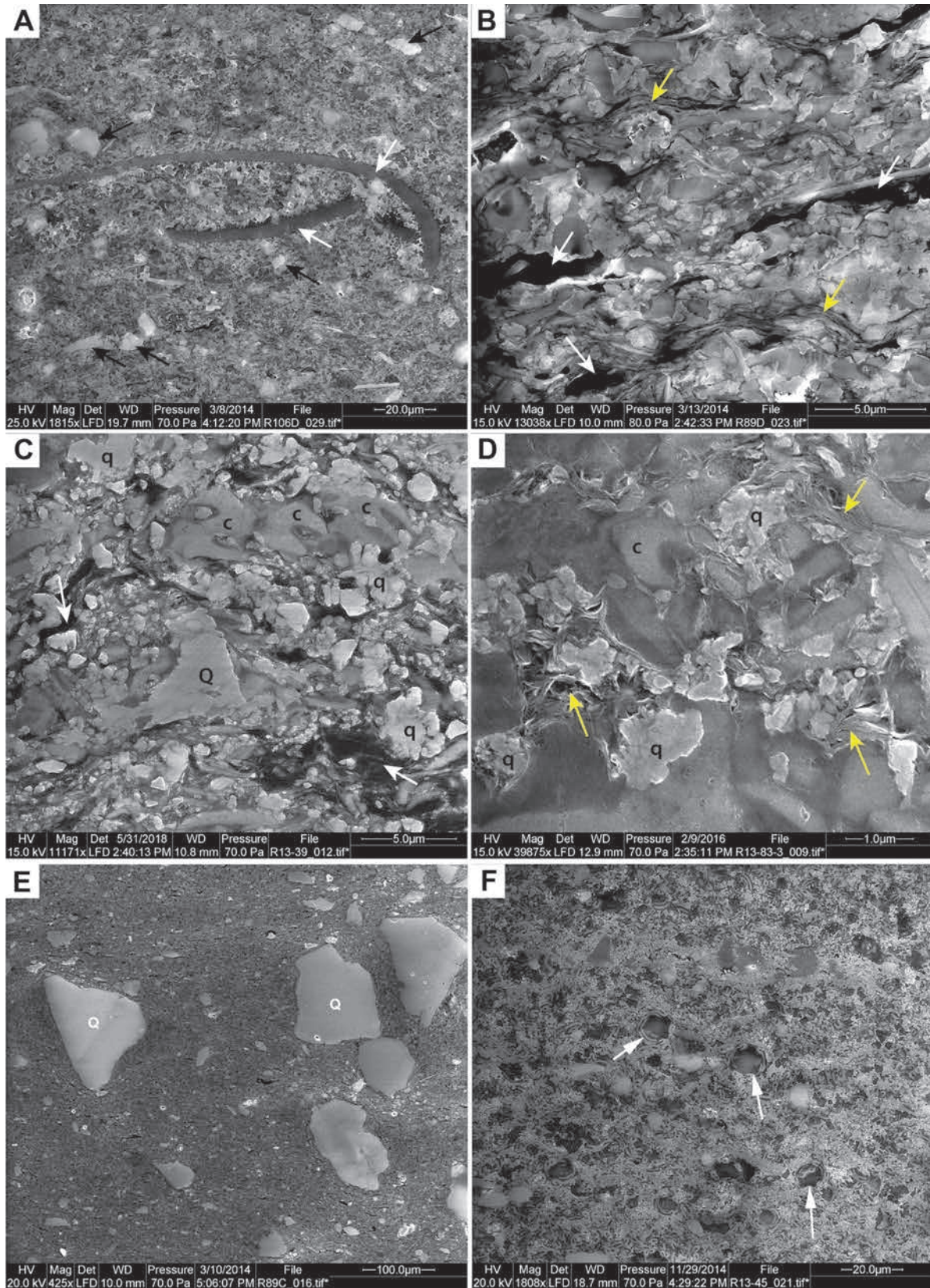
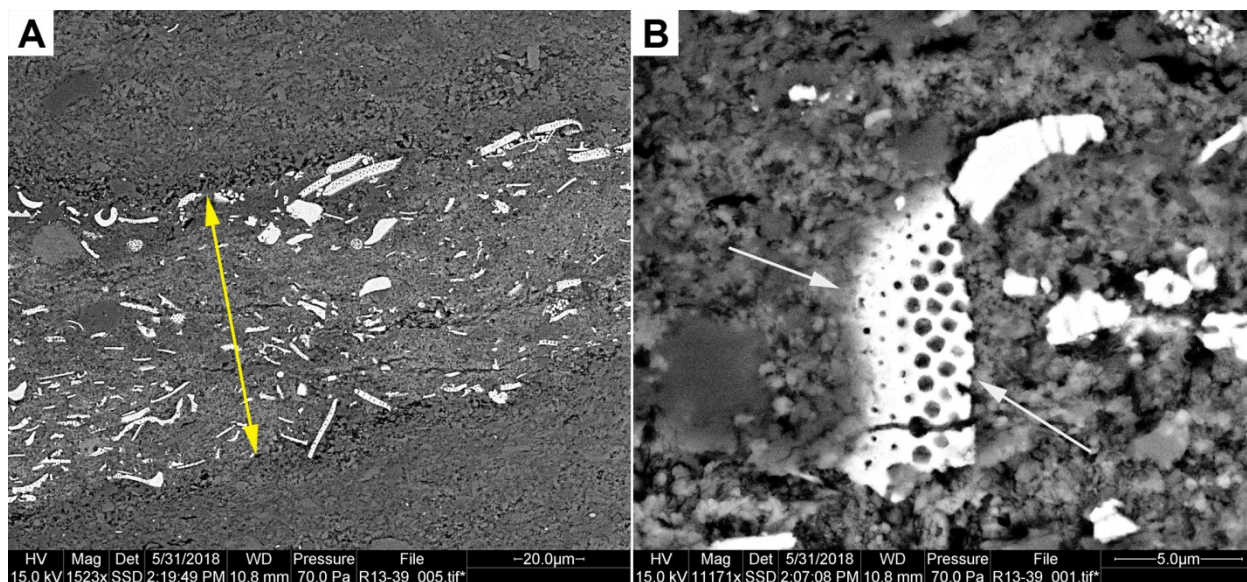**Figure 8**: Key petrographic features of marl beds, see caption on previous page.
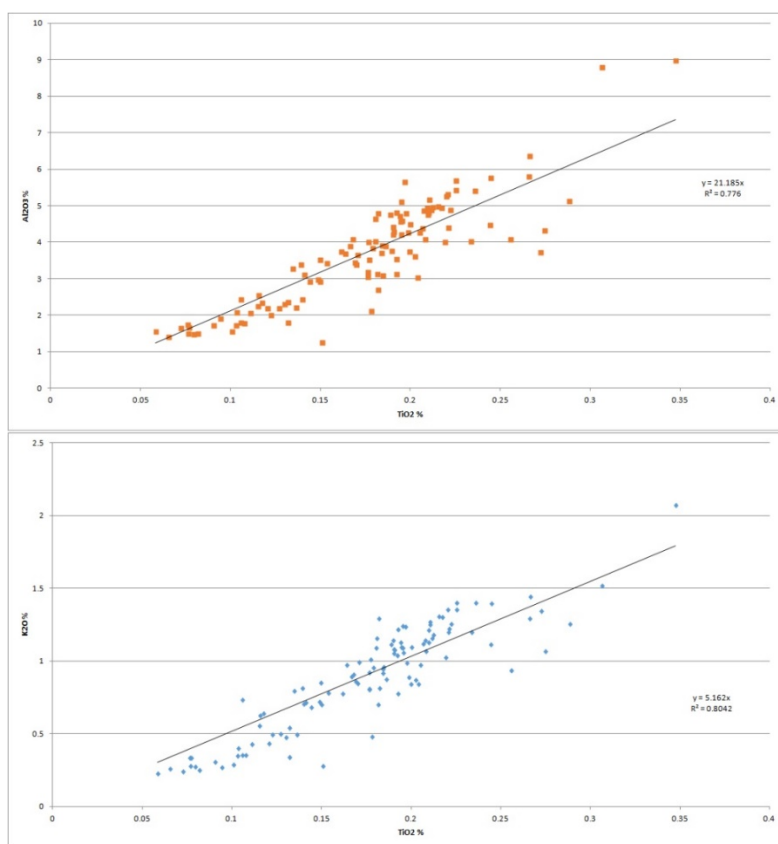
14

Figure D: (A) Portion of a lens that consists of calcareous debris and an abundance of elongate pyrite particles (lens marked by double arrow). The latter show cross-sections typical for diatom frustules. (B) At higher magnififcation the pyrite particles (arrows) show the hexagonal valve structure common to many diatoms.

3.3. Chemical Composition

Spot analyses made with a portable X-ray spectrometer (16 samples; 110 layers) show that Al, K, and Ti show good correlation (Fig. 9) and that there are no apparent compositional groupings.

Figure 9: Scatter plot of XRF data for BMF layers. Shows well developed correlations between Al_2O_3, K_2O, and TiO_2 that suggest that these three elements represent terrigenous input.

With Al_2O_3, K_2O, and TiO_2 as plausible terrigenous clastic proxies, and calcite (approximated as CaO) a presumed biogenic component, a plot of CaO/Al_2O_3 against TiO_2 is also informative in that it shows a negative correlation between the biogenic/clastic ratio and the amount of clastic input (Fig. 10). The plot suggests that rock composition is due to mixing between a clastic (clay, silt) and a pelagic (calcite) end member. The lack of compositional groupings supports the view that the BMF as exposed in the study area represents a compositional spectrum between terrigenous and marine (carbonate) end members and that arbitrary subdivision into several facies may not contribute to a better understanding of the BMF.
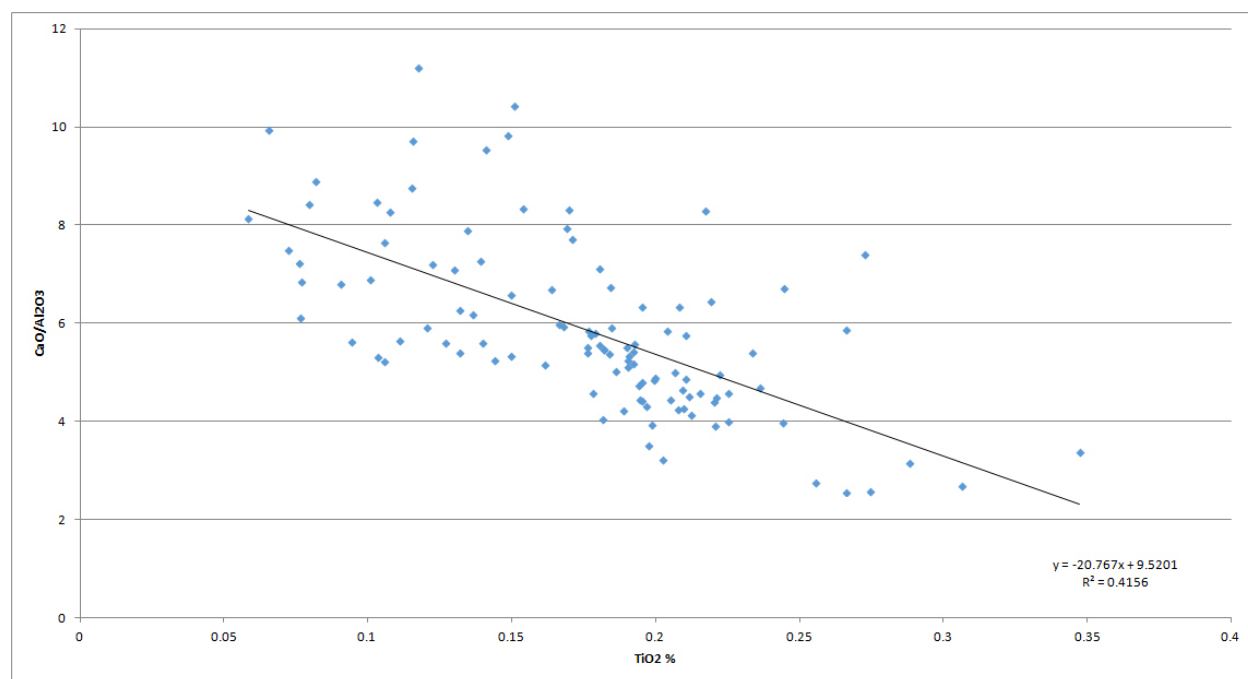

Figure 10: Negative correlation between the biogenic/clastic ratio and total clastic input (TiO_2 as proxy) shows no distinct compositional groupings. The plot also suggests a continuous compositional spectrum between a clastic and a pelagic (calcite) end member.

A plot of SiO_2 versus TiO_2 (not shown) shows a comparable negative correlation as seen for carbonate in Figure 10. The additional lack of positive correlation of SiO_2 with Al_2O_3 and K_2O (not shown) suggests that although detrital quartz is observed under the SEM (Fig. 9), the bulk of the SiO_2 is not terrigenous sourced, but like calcite (pelagic microfossils) is pelagic derived, possibly from dissolved diatoms. The BMF underlying unit contains abundant diagenetically altered diatoms (Puglisi et al., 2006).

3.4. Marl Sedimentary Features - Macroscopic

In multiple places, sedimentary features that allow an estimate of original water content of marl intervals were observed (see above), such as differential compaction around sand filled fissures and load casts (Fig. 4) and deformed and compacted clastic dikes. Many of these indicate water contents on the order of 70 vol % and higher [*extra Figure E*].

Figure E: Differential compaction around a sand-filled scour in the center of the image (hammer handle for scale). The thickness "A" of the sand fill, when compared to convergence of marl layers next to the structure (double arrow "B"), suggests a minimum water content of 75 vol %.

Intervals where thin lenses and layers of sand are interbedded with marly layers may also show cross-lamination within sand lenses (Fig. 11A) and scours at the base of sand lenses. Sand may occur as sub-mm thick laminae, and thin lenses of a few mm thickness may occur with or without associated sand lamina (Fig. 11B). In close-up, sandy layers contain sand-size particles that appear to have been eroded from underlying marl beds (Fig. 11B). Whereas most of these eroded particles are typically less than a mm in size, in places rounded and flattened marl rip-up clasts up to several cm's in size were observed (Fig. 11C), together with concentrations of fish scales on bedding planes (Fig. 11D).
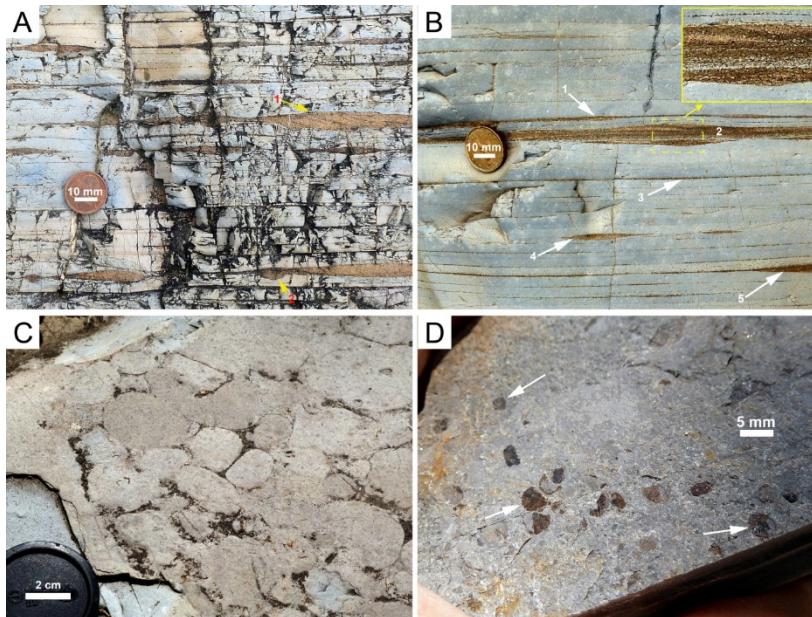

Figure 11: A) Thin sand lenses with cross-laminae (arrow 1) and basal scours (arrow 2). Note that cross-laminae all indicate transport to the right. B) Thin sand laminae with lenticular thickening (arrows 1), of uniform thickness (arrow 3), with cross lamination (layer 2), and single lenses on bedding planes (arrow 4). The enlarged portion of layer two shows gray particles that are of the same appearance as underlying marls. C) Bedding plane with rounded and flattened marl rip-up clasts. D) Bedding plane covered with phosphatic fish scales (brown, arrows).

Although marl layers are generally conformable, in places they can be seen to have discordant basal contacts (Fig. 12). The layer terminations against underlying sand beds, as seen in Figure 12, suggests a lateral transport component for deposition of the marls.
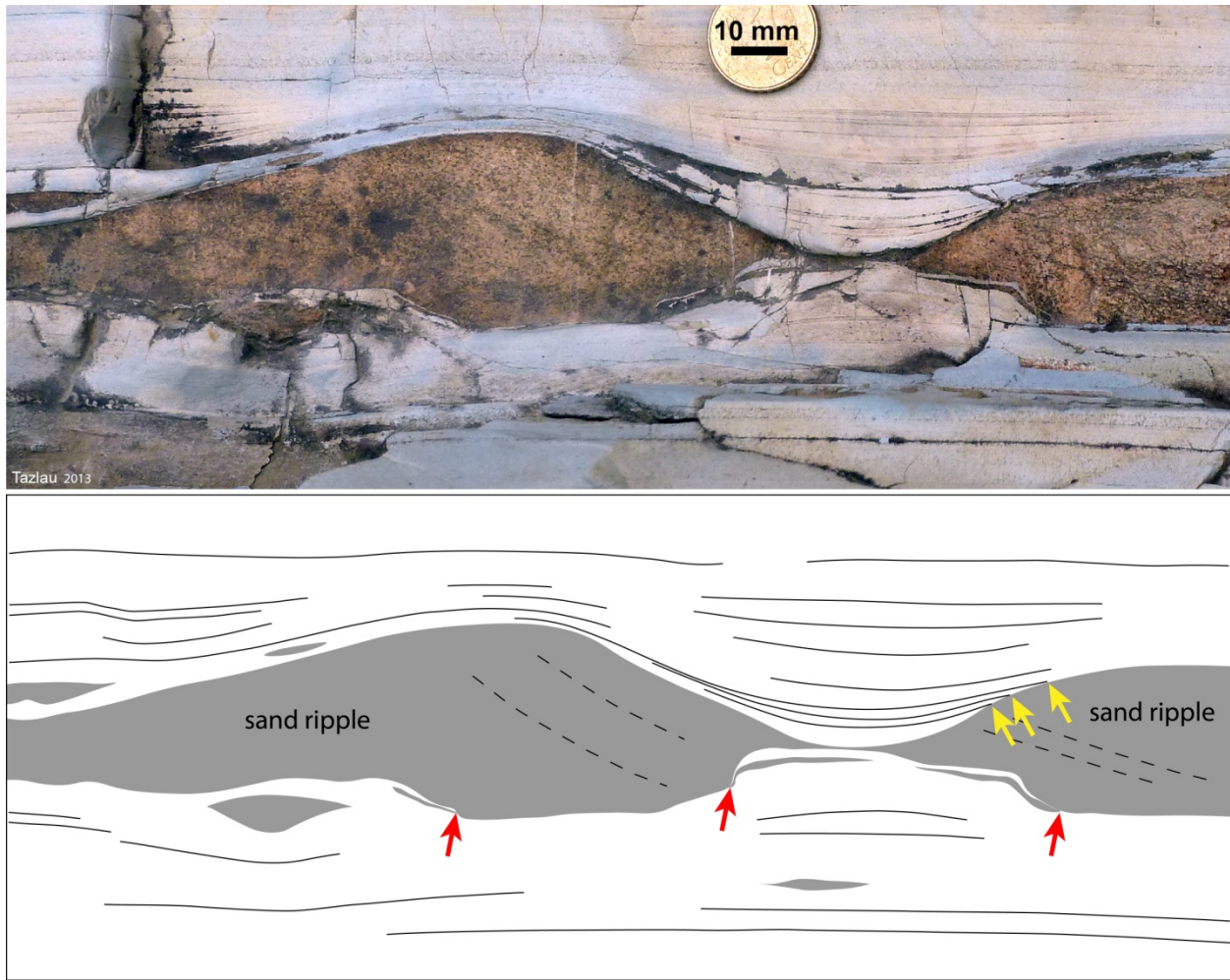
Figure 12: Contact relationship between thin layers of marl and an underlying sand layer. Upper image shows outcrop appearance; lower image is a sketch that highlights layer contacts. Red arrows point to truncated sandy laminae at base of thicker, cross-laminated sandstone lenses, yellow arrows point to marl laminae that terminate on top of sand ripple.

In several places within the BMF outcrops surveyed, macroscopically cross-bedded marls have been observed [*extra Figure F*]. Figure 13 provides a good example of their outcrop appearance.

Figure F: BMF with thin marl layers and a 5 cm thick interval (marked with arrows) that shows cross-stratification.

The foreset orientations suggest a bedform (large ripple) that migrated from the right to the left, and foresets are downlapping onto a basal surface.

The entire bedform was cut out of the outcrop with a concrete saw, embedded in epoxy, and slabbed once returned to the IU Shale Research Lab in Bloomington. This was done to get a clearer look at the bottom and top contact relationships of this bedform, and to ensure that the presumed bedform was not a mere artifact of soft sediment deformation. Figure 13 shows a comparison between the outcrop and its slabbed counterpart. The color difference between the layers that under- and overlie the bedform (layer A in Fig. 13) and the layers that constitute the bedform is due to differences in terrigenous content and diagenetic cements, and possibly bitumen content. The darker color of layer A in Figure 13 reflects a higher terrigenous (clay and silt) component, and the lighter colors of the bedform are due to more calcite and silica cement.
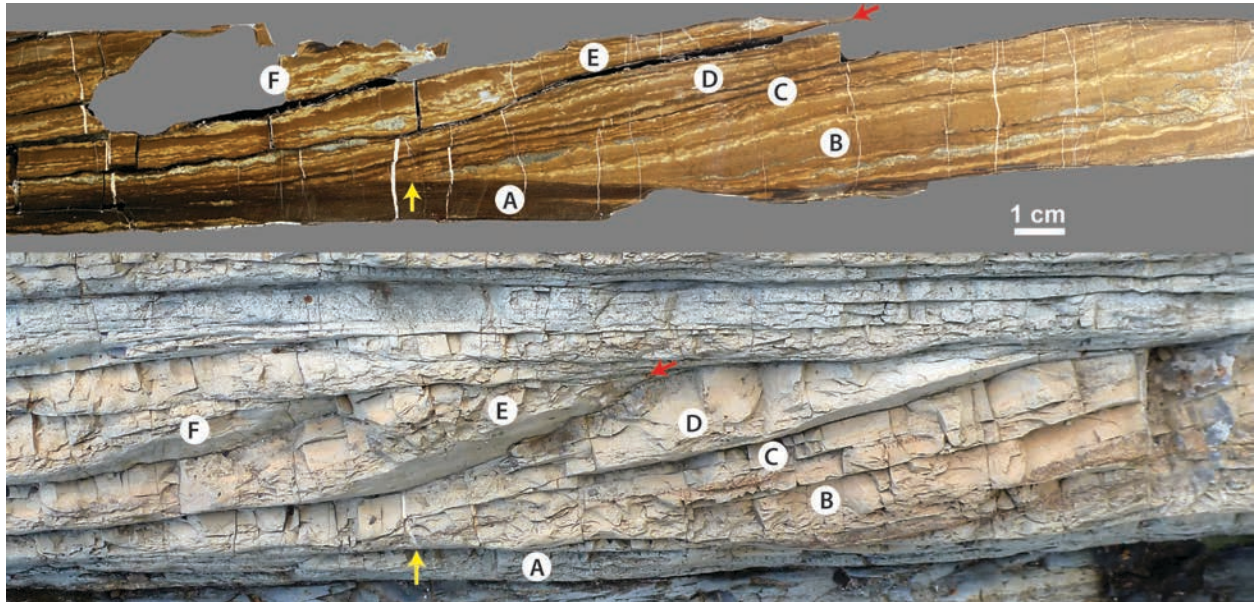

Figure 13: Comparing slabbed sample of mud megaripple (top) to its outcrop equivalent (bottom). Circled letters mark corresponding layers, red and yellow arrows mark corresponding surfaces. In the slabbed sample, the downlap of inclined foresets onto a common surface is clearly visible.

In Figure 13, the contact between the basal layer A and the bedform foresets shows no evidence of dislocation due to shear and soft sediment deformation, it appears to be an undisturbed depositional contact. Likewise, overlying layers are in undisturbed depositional contact with the underlying cross-strata, and the downlapping nature of the cross-beds is evident [*extra Figure G*]. In slabbed slices of this bedform, the cross-beds, as seen in outcrop, show internal layering and soft sediment deformation that suggests downslope movement to the left. Cross-bed inclination measured on these slabs ranges from 8 to 12 degrees. Under assumption of a 75 vol% pre-compaction water content, an average inclination of 10 degrees would translate into 35 degrees of inclination for an uncompacted bedform, and the bedform itself would have a relief of about 20 cm.
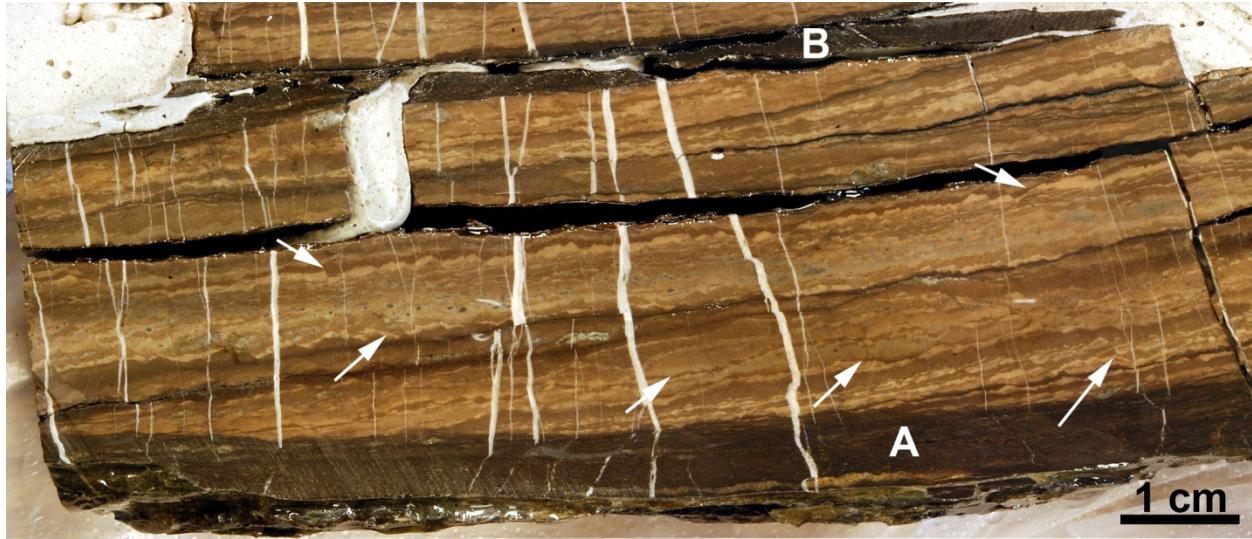
Figure G: Partial image of the slabbed sample produced from the bedform shown in Fig. 13. The basal (layer A) and top (layer B) contacts appear to be depositional and show now indication of shearing or slumping by slope forces. White arrows point to examples of in-bed soft sediment deformation that suggests creep and downslope motion to the left.

3.5. Marl Sedimentary Features - Microscopic

As seen in Figures 6 and 7, the marly intervals of the BMF consist of three components, calcitic layers (abundant coccolith debris, Fig. 8), sandy layers, and marly layers. When examined in detail (Fig. 14), the sand component can occur as thin laminae and lenses that occur at the base of marl layers (sb) or within them (sob), or as dispersed sand grains within a marl matrix.
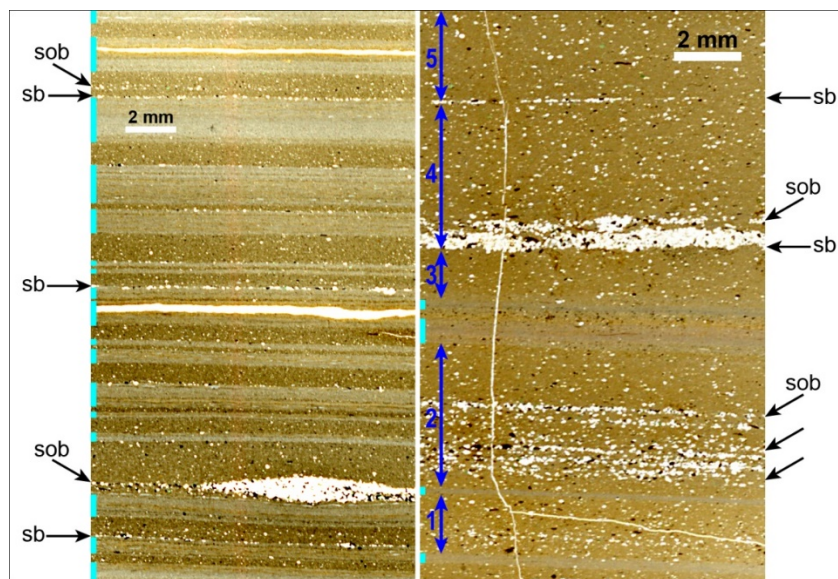

Figure 14: Layering within marly intervals. At left, a sample where marl layers and calcitic layers (light blue markers) alternate, and where sand may occur as very thin concentrations at the base of marl layers (sand at base = sb), or also as layers and lenses within marl layers (sand above base – sob). Dispersed sand grains are a typical component of all marl layers. At right a sample with thicker marl layers and intervening calcitic layers (light blue markers). Specific marl layers marked with blue double arrow and

20

numbered. Layer 1 – shows dispersed sand grains (mostly quartz) in a marl matrix (see Fig. 8E).
Layer 2 shows multiple thin sand-enriched laminae within the marl layer (sand above base –
sob). Layer 3 – dispersed sand grains in marl matrix. Layer 4 – has thin sandy layer at base (sb)
and a thin sandy lamina within the marl (sob). The rest of layer 4 shows sand grains dispersed in
a marl matrix. Layer 5 has a single grain layer of sand at base (sb) and consist otherwise of sand
grains dispersed in a marl matrix.

At higher magnification, the marl consists of deformed lenticular features that range in length
from several ten microns to several hundred microns [*extra Figure H*]. These lenticular features
are in detail fine grained aggregates of diverse composition (Fig. 15). They were soft and
deformable when deposited, and probably were initially eroded from multiple mud substrates
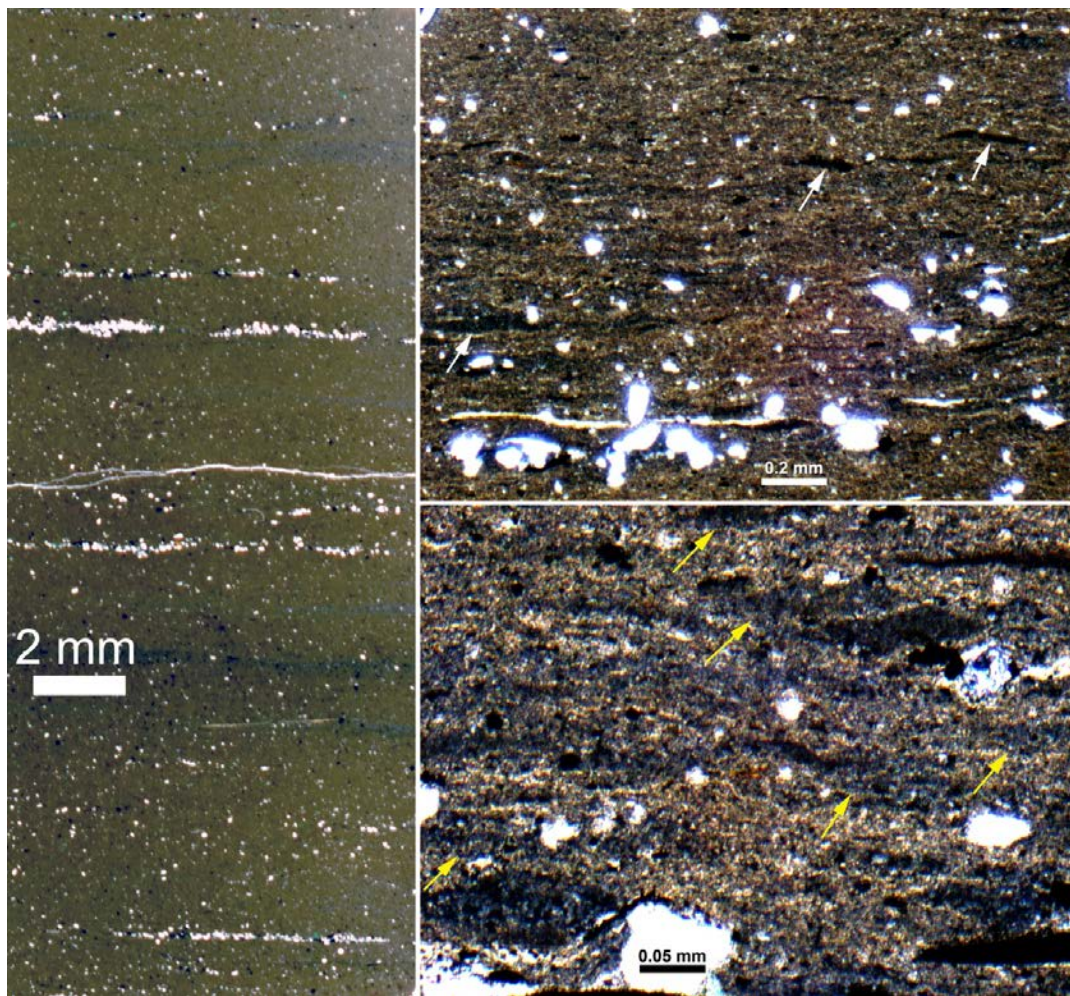available at the seafloor.

*Figure H: Detail of marl layers. At left, portion of thin section with marl layers and thin sandy
lamina and lenses. At right, closer view of marl matrix with dispersed sand grains at increasing
magnification. Upper right, arrows point to examples of thin, darker colored, lenticular features.
Lower right, at higher magnification we see that the marl largely consists of deformed lenticular
features, most of which are too faint (yellow arrows) to be easily visible at lower magnification.*
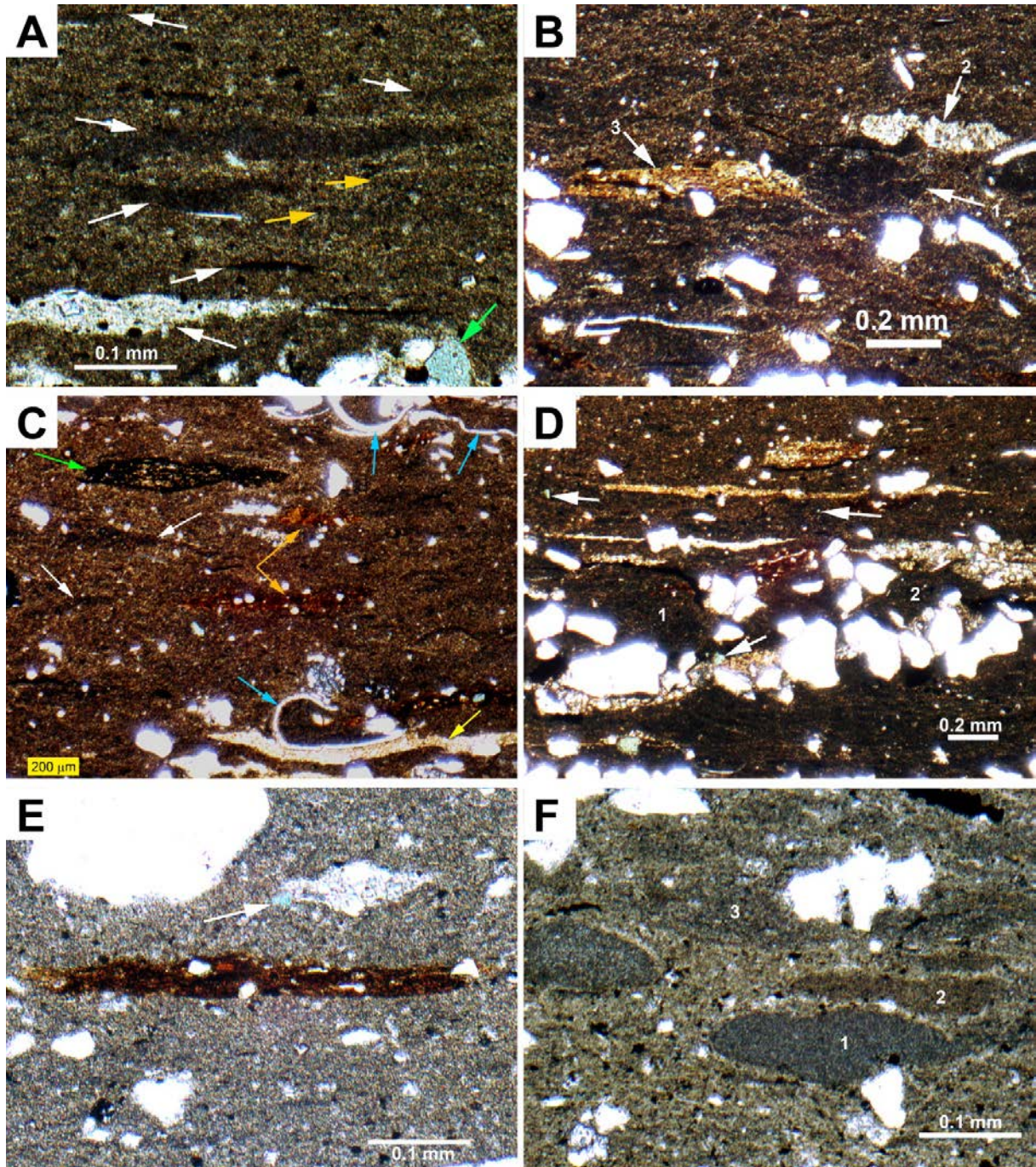
21

Figure 15: A diversity of fine grained aggregate lenses within marl layers. (A) Darker and lighter deformed lenses, consisting of the same material as underlying marl layers. Green arrow points to glauconite. (B) Dark lenses (1) as well as light clay-silt aggregates (2), and brownish clay-organic matter aggregates (3). (C) Multiple aggregate types (arrows) and shell fragments (blue arrows) form a lenticular fabric. (D) Same aggregate types as in (B), some of them squeezed and deformed between sand grains. Arrows point to glauconite. (E) Brownish aggregate with abundant clay and organic matter. Arrow points to glauconite. (F) Three different types of lenses, "1" is calcite rich and consists largely of coccoliths [*extra Figure I*], "2" and "3" consist of the same material that constitutes the general marl matrix (Fig. 8).
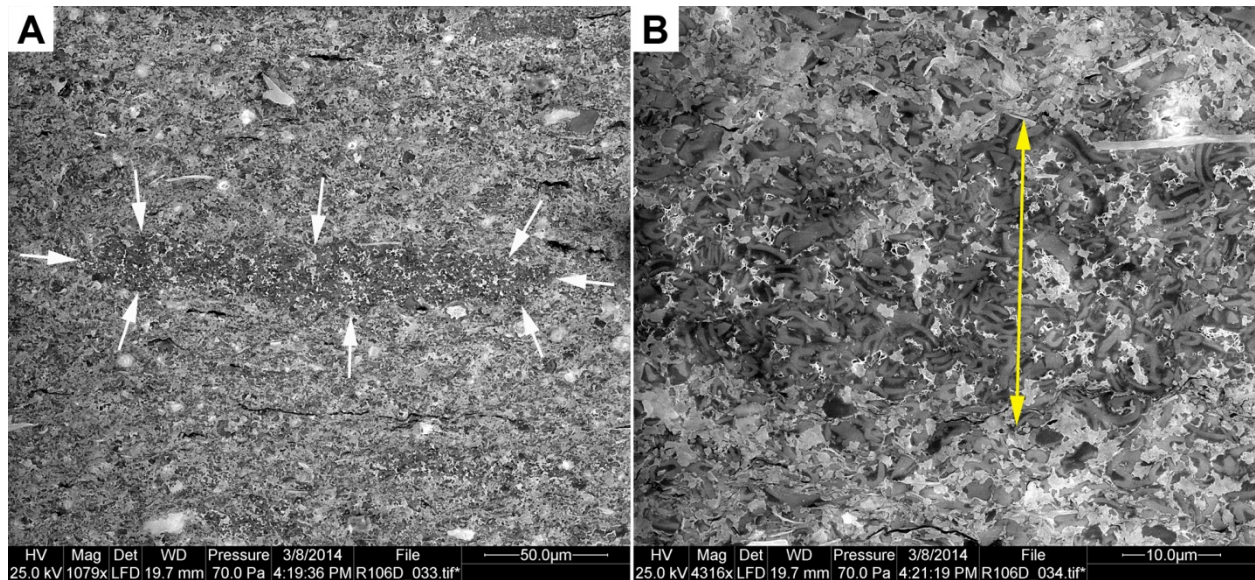
Figure I: (A) SEM image of ion milled marl layer with lens shaped calcite-rich feature (arrows) that consists (B) largely of coccolith debris. In (B), yellow double arrow marks lens shaped feature from (A).

Calcite-rich layers that separate marl layers (Fig. 14) consist of closely packed coccolith debris lenses [*extra Figure J*], which most likely represent planktonic fecal pellets (Schieber et al., 2016; Li and Schieber, 2019). The lighter material in between these lenses consists of a coccolith-rich matrix that may contain preserved coccolithospheres. These layers are lighter than marl layers because they largely consist of coccolith lenses in a matrix of more coccoliths.

When compared to other fine grained aggregate lenses, coccolith lenses tend to be a bit thicker and have lateral terminations that are more rounded instead of tapering. In contrast, lenses that represent general marl rip-ups, though also containing coccolith debris, have an overall more complex composition with added clays and quartz silt grains, as illustrated for example in Figure 8D.
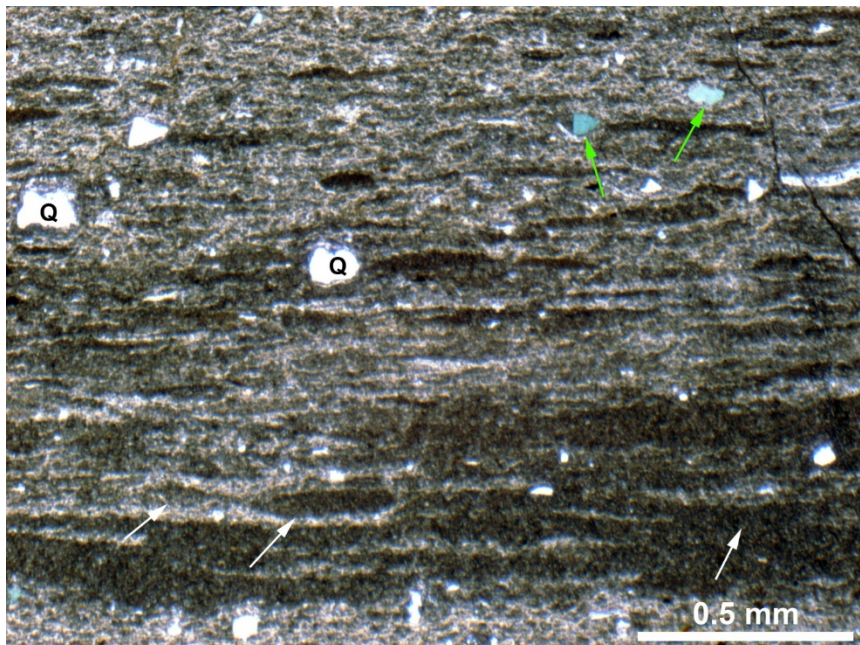
Figure J: Detail of a calcite-rich layer. It consists of abundant closely packed calcite-rich lenses like those shown in Fig. 27 (white arrows). White grains are quartz (Q), and green grains are glauconite (green arrows).

Another, comparatively common calcareous lens type contains variable amounts of diagenetic ferroan dolomite (Fig. 16). These lenses can be so dolomitic as to give the impression of a carbonate grain (Fig. 16A), but the dolomite grains grew within clay-organic aggregates such as shown in Figure 15E. There is a compositional range from aggregates that consist almost exclusively of dolomite grains and those where dolomite grains are scattered through a clay-organic matrix (Fig. 16B).
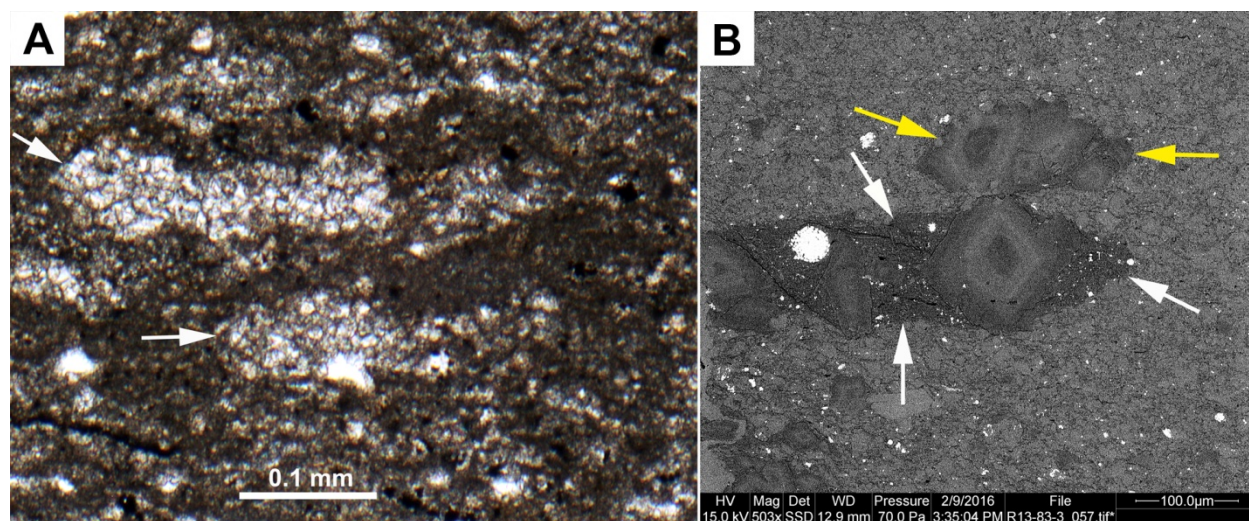

Figure 16: Views of dolomitic lenses within a marl layer. (A) Thin section view of light dolomitic lenses (arrows) that may at first appear to be carbonate grains. (B) SEM view (backscatter) that shows one of these lenses (white arrows) where zoned ferroan dolomite rhombs (zoning due to variable Fe-content) occur within a matrix of clay and organic matter. Another lens (marked with yellow arrows) appears to consist only of dolomite rhombs, although a closer look shows that there still is interstitial clay and organic matter that is identical to that seen in the lens that is marked with white arrows.

All lenses show deformation that suggests that they were soft water-rich particles at the time of deposition, a quality that is most notable when they are next to undeformable sand grains [*extra Figure K*]. Differential compaction next to sand grains suggests that the fine grained aggregate lenses seen in Figure 15 had water contents on the order of 75 vol % or higher.

In places where sand grains are mingled with fine grained aggregates (such as Fig. 5), the aggregates deform to fit in between the sand grains, attesting to their softness and high water content. Aggregates may be indented by sand grains (Fig. 17), but tend to resist complete "puncture", an observation that attests to their internal cohesion and their ability to resist disaggregation during transport.
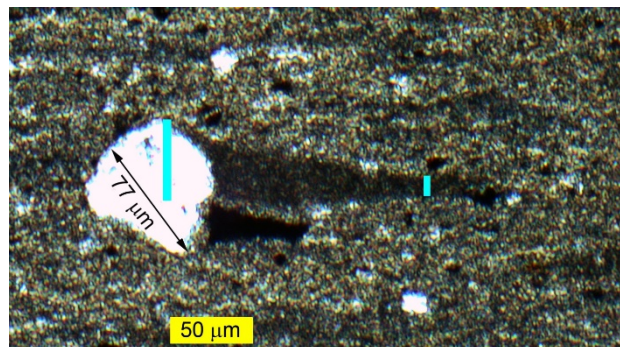

Figure K: Differential compaction of dark fine grained aggregate next to grain of quartz sand. The turquoise bar at left marks the uncompacted thickness, and that on the right shows the compacted thickness, indicating 75 % compaction or 75 vol % initial water content.
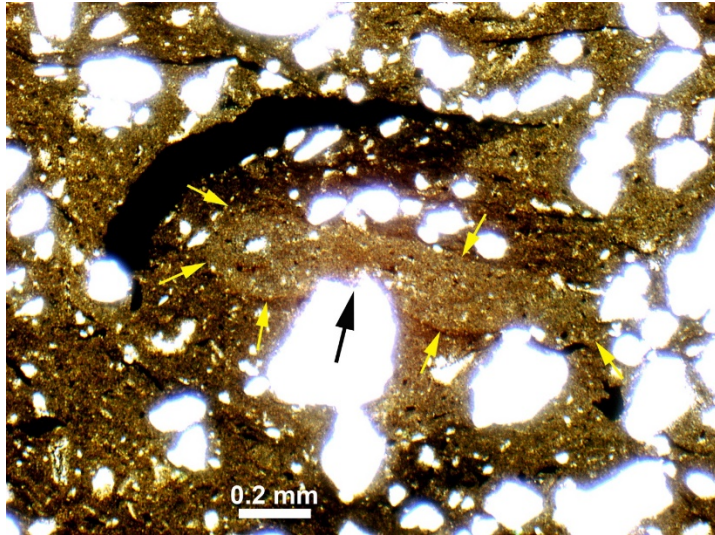
24

Figure 17: A mixture of fine grained aggregates/lenses and sand grains (white). The lens in the center (outlined by yellow arrows) is indented by a quartz grain (black arrow). Due to internal cohesion the lens resisted "puncture" by the quartz grain during compaction.

In several thin sections, elongate particles ("lenses", fossil debris, large mica flakes, etc.) and alignments of particles show a consistent orientation relative to the base of the layer, a phenomenon that one may describe as "inclined fabric elements". Figure 18 provides an example of this feature, and in a given layer it can be observed across the entire width of the thin section [*extra Figures L and M*].

Figure 18: Inclined fabric elements. Upper half shows a photomicrograph of a marl layer with a sharp base and inclined and aligned elongate particles. Most of the latter are dolomitic lenses as shown in Figure 16. Lower half shows a tracing of the perceived inclinations and alignments (yellow dashed lines), and the lower boundary of the layer as a red line. The inclination is to the right at approximately 14 degrees relative to the basal surface (red line).
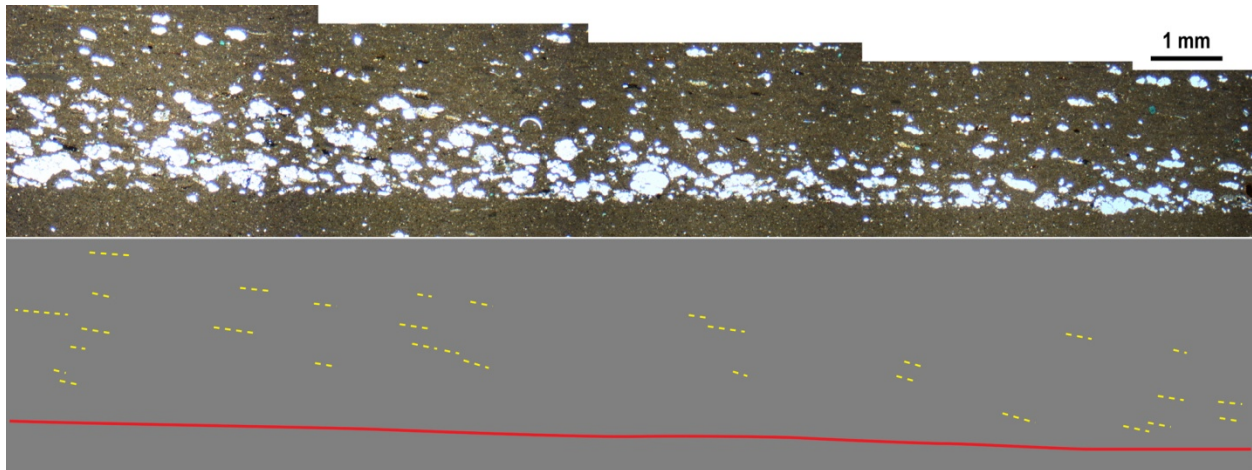
25

Figure L: Inclined fabric elements for the same layer as shown in Fig. 32, but across the entire width of a thin section. Although locally the inclination may measure as steep as 14 degrees (Fig. 32), overall inclination is on the order of 7 to 10 degrees relative to the basal surface.

Figure M: Inclined "sandy" laminae (yellow arrows) at base of marl layer that consist largely of light colored dolomitic lenses (see Fig. 29) and darker fine grained aggregates/lenses (some pointed out by green arrows) like those seen Fig. 26A. These laminae dip towards the left and downlap onto the basal surface. The upper portions of the marl layer show the same inclination (6 degrees relative to the basal surface) to the left as indicated by the orientation of phosphatic fish scales (some pointed out by white arrows).

In a few thin sections, mm-thick layers of carbonaceous mudstone were observed that consist of abundant wavy-anastomosing carbonaceous-kerogenous laminae (Fig. 19). A portion of these carbonaceous laminae can be traced across the width of thin sections. They do not seem to contain particulate organic matter (such as alginite and chitin debris) and are interlayered with lenses and thin laminae that consist of the same clay-silt-coccolith mixture that is typical for marl beds. The carbonaceous lenses that have been observed in thin sections (Fig. 15B and 15E) resemble these layers and appear to have been derived from them.

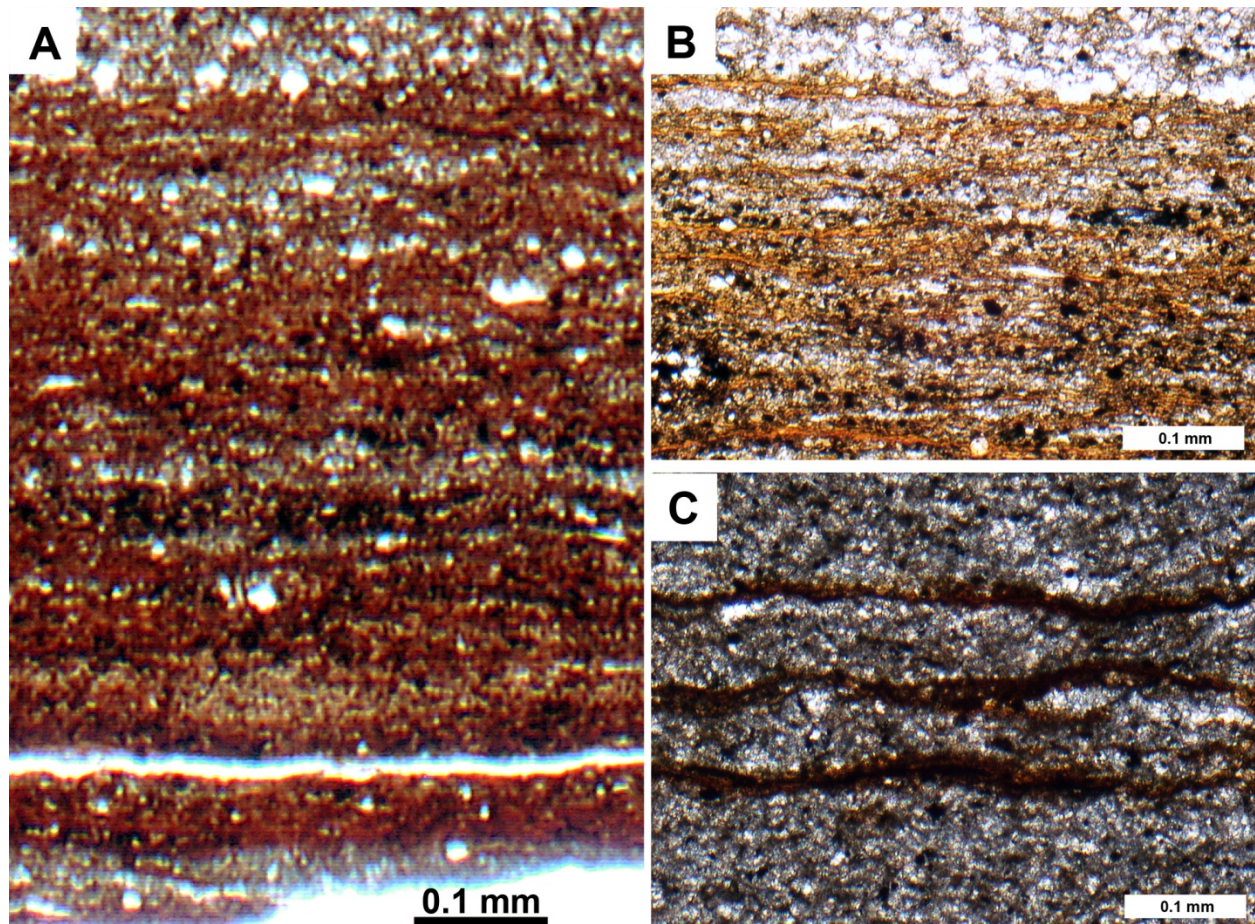**Figure 19**: Photomicrographs of wavy kerogen laminae in carbonaceous mudstone layers. (A) A thin layer with abundant wavy-anastomosing kerogen laminae (reddish brown). (B) Another view of kerogen laminae that better shows wavy-anastomosing texture. (C) Continuous wavy kerogen laminae separated by thin layers of marl matrix.

4. Interpretation of Sedimentary Features and Textures

At the outcrop scale, the presence of sandy intervals with ripple cross-lamination (Figs. 4, 11, 12) is a first indication that bottom currents transported sediment across the seabed. The common presence of load casts (Fig. 4) and differential compaction around sandy scour and fissure fills, suggesting water contents of 70 vol % and more, attests to a water-rich surficial mud substrate. Variable intensity of sediment loading over small vertical distances (Fig. 4) indicates variable water content of surface sediment, possibly reflecting differences in sedimentation rate, with more watery layers deposited more quickly. Scouring of the mud substrate (Figs. 12) and mud rip-up clasts (Fig. 11) indicate bottom currents in excess of flow velocities needed for mere sand transport (Hjulström, 1939; Sundborg, 1967; Reineck and Singh, 1980). Cross-bedded marls like those seen in Figure 13 suggest that bedload transport of mud gave rise to megaripples (sensu Reineck and Singh, 1980). They will be discussed in more detail below, after consideration of depositional processes for marl layers.

The soft sediment deformation features shown in Figure 3 suggest downslope gravitational

transport of soft mud-rich strata. Some, like layers with convolute bedding (Fig. 3A) and floating blocks (Fig. 3B) can be regarded as classical slump deposits (e.g. Allen, 1985), whereas unconformable contacts (Fig. 3C) are probably slide planes where large blocks of semi-consolidated sediment slid across the surface. Disturbed bedding seen in Figure 3E may record incipient creep by gravitational pull on slope deposited sediments. The presence of slump features in these strata have previously been reported by Miclăuș et al. (2009). Because these slumped deposits include marls that also form the remainder of the BMF, they imply that portions of the BMF were deposited in a slope setting.

   Because sandy turbidities seem absent in the BMF, one may wonder where the cross-laminated sand in Figures 4 and 11 originated. The glauconite pellets that occur within the sand layers (Fig. 5) suggest derivation from a warm shallow water setting, possibly nearshore and in proximity of freshwater input (Triplehorn, 1966; Odin, 1988; Harding et al., 2014). Given that the slump deposits typically contain a substantial sand component (with glauconite), slumps can be considered a likely mechanism for sediment transfer from the shelf to the base of slope. Once slump lobes came to rest at the base of the slope, reworking of these deposits by bottom currents provided the sand component of the BMF marl intervals, an inference that is supported by the common observation of glauconite in marl layers (Fig. 15).

   Considering the high content of planktonic fossil debris in marl beds (Fig. 8), one could interpret them as pelagites and assume that marl beds formed as planktonic organisms and fecal pellets settled through the water column and accumulated at the seafloor. Indeed, the calcite-rich layers that are interbedded with marl layers (Figs. 7, 14) could certainly be interpreted as the result of simple pelagic settling. Yet, the presence of scattered grains of quartz sand and glauconite shows that these layers received a terrigenous component in addition to pelagic input. Because sand size quartz grains will settle out of river plumes close to the shoreline, the sand grains in calcite-rich layers most likely arrived in the deeper portions of the basin via a combination of bottom currents (across shelf) and slumping.

   The abundance of diverse fine grained aggregate lenses within marl layers (Fig. 15) is not consistent with a simple suspension settling origin. These lenses have long axis dimensions of 100 microns or more, were soft and deformable at the time of deposition, had water contents on the order of 75 vol % or more, and the marl layers show lenticular fabric (Schieber et al., 2010) under the microscope. With the exception of planktonic fecal pellets, these lenses appear to have been derived from soft water-rich muds that were present at the seafloor. This interpretation is supported by comparison with modern surficial marine muds, which have water contents in the 70 to 90 vol % range in the uppermost decimeter (Terwindt and Breusers, 1972; Schimmelmann and Lange, 1996). Lenticular fabric was first described from the Proterozoic Rampur Shale (Schieber et al., 2007b) and interpreted as re-deposited particles that had been eroded by bottom currents. Subsequent flume experiments demonstrated that erosion of water-rich muds generates sand-size and rounded soft rip-ups that can be transported for substantial distances by bottom currents (Schieber et al., 2010). Once redeposited, these rounded soft particles are flattened by compaction and give rise to lenticular fabric. That the envisioned scenario is probably a rather common process on muddy seabeds is suggested by recent reports of lenticular fabric from multiple shale successions in the rock record that are consistent with bottom current reworking (e.g. Davies et al., 2012; Kietzmann et al., 2014; Könitzer et al., 2014; Laycock et al., 2017; Newport et al., 2018).

   When looked at with high magnification, BMF thin sections readily show flattened lenses or mud-rip ups (Fig. 15), but one also sees lighter material between more obvious lenses. Some of

this lighter material can be resolved as lenses of lighter color at even higher magnification, but one has to wonder about the nature of the unresolvable residual. From experimental work we know that the stable transport velocity/shear stress range for rip-ups (Schieber et al., 2010) coincides with the velocity range where mud floccules are stable during bedload transport (Schieber et al., 2007a; Schieber, 2011). Given that both floccules and rip-ups have similar water contents, with ca. 85-90 vol % for floccules and 70-85 vol % for rip-ups, and are similar in size (Schieber et al., 2007a; Schieber et al., 2010; Schieber, 2011), it is plausible that in addition to rip-up aggregates, flocculated mud was carried across the seabed by bottom currents as well. Co-transport of flocculated muds and soft rip-ups could explain the lighter "residual" between the more recognizable flattened rip-up aggregates.

Flocculated muds form ripples in the course of bedload transport (Schieber et al., 2007a) and can show cross-laminae in flume studies (Schieber and Southard, 2009; Schieber et al., 2013), which are liable to give the appearance of planar-parallel lamination upon compaction. In the rock record, non-parallel lamina geometry and basal downlap provide important clues for the identification of mud beds that accumulated via migrating floccules ripples (Schieber and Yawar, 2009; Schieber, 2011; Lazar et al., 2015; Schieber, 2016). One may wonder in that context whether bedload transport of sand size water-rich rip-ups, with or without admixed flocculated mud, might form ripples as well and preserve an imprint of this transport mode. The inclined fabric elements that have been observed in several thin sections of marly layers (Fig. 18) could be a subtle expression of inclined internal layering due to ripple migration. Compacted inclinations against the basal surface are generally between 6 and 10 degrees, which under assumption of 75 vol % water content would translate into foreset dips between 23 and 35 degrees, well within the range observed for floccules ripples in flume experiments (Schieber and Southard, 2009; Schieber, 2011).

Sand grains within marly beds that are dispersed as single grains among the bulk of rip-up aggregates attest on one hand to the cohesiveness of intervening mud rip-ups that prevented these much denser grains to "settle/sink" through the mud component (Fig. 17), and also suggest that these grains were transported together with the mud rip-ups. Thin laminae and lenses of sand within marl layers (Fig. 14) may record intermittent sediment starved conditions where sand grains could congregate into thin patches and veneers, not unlike the formation of coarse silt laminae in silt laminated shales (Yawar and Schieber, 2017). The thin sand laminae at the base of some marl layers may have the same origin, possibly recording preferential deposition of sand at the onset of deposition when flow velocities were still rather high.

Sand grains dispersed in a mud matrix could at first approximation be interpreted as an indication of gravity driven mudflow or debrite deposition (Stow and Piper, 1984; Mulder and Alexander, 2001), but the typical mm-scale thickness of marl layers (Fig. 7) is substantially smaller than reported thicknesses of debris flows (Stow and Piper, 1984; Talling, 2013). Also, it does not seem plausible that such thin sheets of material with sufficient presumed viscosity to support sand grains could have moved any appreciable distance even at slope angles of several degrees. The observation that, internally, marl layers consist of sand size fine grained aggregates instead of a more homogenous clay-rich matrix also seems incompatible with a presumption of laminar and plug flow (Mulder and Alexander, 2001).

Megaripples (sensu Reineck and Singh, 1980) like the one shown in Figure 13 have been observed in multiple locations in the study area, and detailed study of one of them confirms that these are genuine bedforms rather than an artifact of soft sediment deformation. Downlapping geometry of foresets and soft sediment deformation within foresets is consistent with a migrating

bedform that largely consists of water-rich particles. In sandy deposits, the change from small ripples to larger scale bedforms is caused by an increase in flow velocity or stream power (Allen, 1970), but increasing flow velocity is not a viable method for growing larger muddy bedforms. In experiments, both mud floccules and soft rip-ups start to disintegrate and disperse once approximately 25 cm/sec (bottom shear stress about 0.21 Pa) flow velocity is reached (Schieber et al., 2007a; Schieber et al., 2010). Although the dimensions of our flumes for mud sedimentology (Schieber et al., 2007a; Schieber, 2011) are unsuited for replicating mud megaripples in the lab, in some long running experiments exceptionally large ripples were produced, suggesting flow duration as a potential variable. Whether there are definable stability fields for different scales of muddy ripples, analogous to those know from sandy bedforms (Middleton and Southard, 1978), will require further experimental studies.

Carbonaceous mudstones with wavy-anastomosing carbonaceous-kerogenous laminae (Fig. 19) resemble deposits of microbial mats observed elsewhere in ancient mudstone successions (Schieber, 2007). Whereas carbonaceous laminae alone are not considered "strong" evidence for a microbial mat origin, the ability to trace carbonaceous laminae across the width of thin sections, as well the lack of particulate organic matter (alginate, chitin debris, etc.) are suggestive of a microbial mat origin for these laminae. Additional support for this interpretation comes from the presence of thin, elongate, and variably deformed clay-organic aggregates (Fig. 15E, 16B) that suggest cohesive properties in excess of those typical for mere clay layers, because unusual coherence of organic-rich mud rip-ups can be an indication of derivation from a microbial mat substrate (Schieber, 1999).

Collectively, the observed sedimentary features in the marl layers, as well as in associated sandstones, speak to a mobile seabed that was "on the move" for a substantial part of its depositional history. The apparent lack of bioturbation in the BMF and its lateral equivalents has in the past been attributed to anoxic conditions (e.g. Kotlarckzyc and Uchman, 2012), but frequent bottom current reworking and intermittent erosion in an oxygen restricted environment would have had a comparable effect. Slump deposits and soft sediment deformation suggest an overall slope to toe of slope depositional setting. The bottom current activity that is recorded by sand layers and lenses, as well as the marl layers themselves, suggests that current activity dominated the seabed. Development of muddy megaripples may indicate long lasting unidirectional currents and suggests that the marls represent contourite deposits that accumulated in a lower slope to basin floor environment.

5. Conclusions

Substantial portions of the BMF in the Vrancea Nappe of the Eastern Carpathians reflect planktonic components (coccoliths, foraminifera, diatoms, fecal pellets) that initially must have settled through the water column to the seafloor. Bottom currents that swept the seabed and intermittently eroded it probably incorporated these components directly, or remobilized them from their initial muddy deposits in the form of soft rip-up clasts.

The present day marls consist of abundant coarse silt to sand size fine grained aggregates that originated as fecal pellets, soft rip-ups from previously deposited marl beds, as well as soft rip-ups from a diversity of other muddy substrates exposed at the seabed.

The erosive force that generated these rip-ups was provided by bottom current systems that carried these soft rip-ups for substantial distances and mixed rip-ups from several different

muddy substrates, including organic matter enriched benthic microbial mats that grew in areas of low net sedimentation.

These currents also eroded and reworked slump deposits and in that way acquired terrigenous and shelf derived components like clays, quartz and glauconite. Continued current flow mixed these particles with an abundance of soft rip-ups, carried them along the seabed in the form of small bedload ripples, and eventually deposited them in form of thin marl layers. Current flow episodes of unusual duration led to the formation of muddy megaripples, a new bedform category in mudstone sedimentology.

Overall, the BMF records a combination of slope processes and bottom current activity. Collectively, the BMF marls as well as the interbedded sands suggest an environment strongly dominated by current flow, whereas evidence of non-current sediment accumulation (such as microbial mats and pelagic laminae) is sparse. The likely environment of deposition is a lower slope to basin setting where contour currents reworked pelagic deposits and intermittent sediment supply provided by slumping.

Acknowledgements

References

Allen, J.R.L., 1970. A quantitative model of grain size and sedimentary structures in lateral deposits. Geological Journal 7, 129-146.

Allen, J.R.L., 1985. Principles of physical sedimentology. George Allen & Unwin, London.

Anastasiu, N., Popa, M., Vârban, B., 1994. Oligocene turbiditic sequences of the East Carpathians (Romania): facies analysis, architecture and cyclic events. Studii și cercetări de Geologie 39, Academia Română, București, 35-43.

Anastasiu, N., Popa, M., Vârban, B., 1995. Facies analysis on Oligocene formations from Outer Flysch Zone (the East Carpathians); a reconsideration. Geological Society of Greece Special Publication 4, 317-323.

Athanasiu, S., Macovei, G. & Atanasiu, I., 1927. La zone marginale du flysch dans la partie inférieure du bassin de la Bistrița. Guide des excursions. Association pour l'avancement de la géologie des Carpates. Deuxième Réunion en Roumanie. Cultura Românească, București, 315-353.

Balla, Z., 1986. Palaeotectonic reconstruction of the Central Alpine-Mediteranean belt for the Neogene. Tectonophysics 127, 213-243

Bădescu, D., 2005. The tectono-stratigraphic evolution of Eastern Carpathians during Mesozoic and Cenozoic. Editura Economică, București. (in Romanian)

Belayouni, H., di Staso, A., Guerrera F., Martín-Martín, M., Miclăuş C., Serrano, F., Tramontana, M., 2009. Stratigraphic and geochemical study of the organic-rich black shales in the Tarcău Nappe of the Moldavidian Domain (Carpathian Chain, Romania). International

Journal of Earth Sciences (Geol. Rundsch) 98, 157-176.

Davies, S. J., Leng, M. J., Macquaker, J. H. S., Hawkins, K., 2012. Sedimentary process control on carbon isotope composition of sedimentary organic matter in an ancient shallow-water shelf succession. Geochemistry, Geophysics, Geosystems 13, Q0AI04, doi:10.1029/2012GC004218.

DeCelles, P.G., Giles, K.N., 1996. Foreland basin systems. Basin Research 8, 105-123.

Dzulynski, S., Kotlarczyk, J., 1962. On load-casted ripples. Annales de la Societe Geologique de Pologne 32/2, 147–160

Ellouz, N., Roca, E., 1994. Palinspastic reconstructions of the Carpathians and adjacent areas since the Cretaceous: a quantitative approach. In: Roure F. (Ed.) Peri-Tethyan Platforms. Editions Technip, Paris, pp 51-78

Filipescu, M.G., 1934. Conditions of Eastern Carpathians Oligocene deposits' formation. Buletinul Societății Studenților în Științe Naturale 4 (1933), 89-94. (in Romanian)

Grasu, C, Catană, C., Grinea, D., 1988. Carpathian Flysch. Petrography and economic considerations. Editura Tehnică, București. (in Romanian)

Grasu, C., Catană, C., Miclăuș, C., Boboș, I., 1999. Eastern Carpathians Molasse. Petrology and Sedimentogenesis. Editura Tehnică, București. (in Romanian).

Guerrera, F., Martín-Martín, M., Martin-Rojas, I., Miclăuș, C., Serrano, F., Martín-Pérez, J.A., 2012. Tectonic control on the sedimentary record of the central Moldavidian Basin (Eastern Carpathians, Romania). Geologica Carpathica 63, 463-479.

Harding, S.C., Nash, B.P., Petersen, E.U., Ekdale, A.A., Bradbury, C.D., Dyar, M.D., 2014. Mineralogy and Geochemistry of the Main Glauconite Bed in the Middle Eocene of Texas: Paleoenvironmental Implications for the Verdine Facies. PLoS ONE 9(2): e87656. doi:10.1371/journal.pone.0087656

Hjulström, F., 1939. Transportation of debris by moving water. In: Trask, P.D. (Ed.), Recent marine sediments: a symposium. American Association of Petroleum Geologists. Tulsa, Oklahoma. pp. 5-31.

Kietzmann, D.A., Palma, R.M., Riccardi, A.C., Martín-Chivelet, J., López-Gómez, J., 2014. Sedimentology and sequence stratigraphy of a Tithonian–Valanginian carbonate ramp (Vaca Muerta Formation): A misunderstood exceptional source rock in the Southern Mendoza area of the Neuquén Basin, Argentina. Sedimentary Geology 302, 64-86.

Kotlarczyk, J., Uchman, A., 2012. Integrated ichnology and ichthyology of the Oligocene Menilite Formation, Skole and Subsilesian nappes, Polish Carpathians: A proxy to oxygenation history. Palaeogeography, Palaeoclimatology, Palaeoecology 331-332, 104-118.

Könitzer, S.F., Davies, S.J., Stephenson, M.H., Leng, M.J., 2014. Depositional Controls On Mudstone Lithofacies In A Basinal Setting: Implications for the Delivery of Sedimentary Organic Matter. Journal of Sedimentary Research 84, 198-214.

Laycock, D.P., Pedersen, P.K., Montgomery, B., Spencer, R.J., 2017. Identification, characterization, and statistical analysis of mudstone aggregate clasts, Cretaceous Carlile Formation, Central Alberta, Canada. Marine and Petroleum Geology 84, 49-63.

Lazar, R., Bohacs, K.M., Schieber, J., Macquaker, J., Demko, T., 2015. Mudstone Primer: Lithofacies variations, diagnostic criteria, and sedimentologic/stratigraphic implications at lamina to bedset scale. SEPM Concepts in Sedimentology and Paleontology #12, Tulsa, Oklahoma.

Li, Z., and Schieber, J., 2019, Detailed Petrographic Studies of the Late Cretaceous Tununk Shale Member of the Mancos Shale Formation: Prevalence and Types of Mud-Dominated

Composite Particles in Mudstones. Journal of Sedimentary Research, in press.

Mastalerz, M., Schieber, J., 2017. Effect of ion milling on the perceived maturity of shale samples: Implications for organic petrography and SEM analysis. International Journal of Coal Geology 183, 110-119.

Maţenco, L., 2017. Tectonics and exhumation of Romanian Carpathians: Inferences from kinematic and thermochronological studies. In: Rădoane, M., Vespremeanu-Stroe, A. (Eds.), Landforms Dynamics and evolutions in Romania. Springer Geography, pp. 15-56.

Mărunţeanu, M., 1999. Litho- and biostratigraphy (calcareous nannoplankton) of the Miocene deposits from Outer Moldavides. Geologica Carpathica 50/4, 313-324.

Melinte, M.C., Jipa, D., Rădan, S., Brustur, T., Szobotka, S.A., 2002. K/T boundary event in the Romanian Carpathians. Geologica Carpathica 53, Special Issue, Bratislava.

Melinte-Dobrinescu, M., Jipa, D.C., Brustur, T., Szobotka, S., 2008. Eastern Carpathian Cretaceous Oceanic red beds: lithofacies, biostratigraphy, and paleoenvironment. In: Hu, X., Wang, C., Scott, R.W., Wagreich, M., Jansa, L. (Eds.), Cretaceous oceanic red beds: stratigraphy, composition, origins, paleooceanographic, and paleoclimatic significance. SEPM Special Publication 91, pp. 119-127.

Miclăuş, C., Loiacono, F., Puglisi, D., Baciu, D.S., 2009. Eocene-Oligocene sedimentation in the external areas of the Moldavide Basin (Marginal Folds Nappe, East Carpathians, Romania); sedimentological, paleontological and petrographic approaches. Geologica Carpathica 6/5, 397–417.

Micu, M., 1976, Geological map of Romania. Sheet 48b Piatra Neamţ. Institute of Geology and Geophysics. Geological Atlas 1:50,000. Romania.

Micu, M., Gheţa, N., 1986. Eocene-Oligocene boundary in Romania on calcareous nannoplankton. Dări de Seamă ale Institutului de Geologie şi Geofizică 70-71/4 (1983, 1984), 289-307.

Middleton, G.V., Southard, J.B., 1978. Mechanics of Sediment Movement. SEPM Short Course 3, Tulsa, Oklahoma.

Mulder, T., Alexander, J., 2001. The physical character of subaqueous sedimentary density flows and their deposits. Sedimentology 48, 269-299.

Mutihac, V., 1992. Geological structure of Romania' territory. Editura Tehnică, Bucureşti. (in Romanian)

Newport, S.M., Jerrett, R.M., Taylor, K.G., Hough, E., Worden, R.H., 2018. Sedimentology and microfacies of a mud-rich slope succession: in the Carboniferous Bowland Basin, NW England (UK). Journal of the Geological Society 175, 247-262.

Odin, G.S., 1988. Green Marine Clays: Oolitic Ironstone Facies, Verdine Facies, Glaucony Facies and Celadonite-Bearing Facies - A Comparative Study. Elsevier, Amsterdam.

Pettijohn, F.J., 1957. Sedimentary Rocks. Harper. New York.

Plint, A.G., Macquaker, J.H.S., Varban, B.L., 2012. Shallow-water, storm-influenced sedimentation on a distal, muddy ramp: Upper Cretaceous Kaskapau Formation, Western Canada foreland basin. Journal of Sedimentary Research 82, 801-822

Puglisi, D., Bădescu, D., Carbone, S., Corso, S., Franchi, R., Gigliuto, L.G., Loiacono, F., Miclăuş, C., Moretti, E., 2006. Stratigraphy, petrography, and palaeogeographic significance of the Early Oligocene "menilite facies" of the Tarcău Nappe (Eastern Carpathians, Romania). Acta Geologica Polonica 56/1, 105-120.

Reineck, H.E., Singh, I.B., 1980. Depositional Sedimentary Environments. Springer, Berlin.

Roure, F., Roca, E., Sassi, W., 1993. The Neogene evolution of the outer Carpathians flyschs

units (Poland, Ukrainia and Romania): Kinematics of a foreland/fold-and-thrust belt system. Sedimentary Geology 86, 177-201.

Rowe, H., Hughes, N., Robinson, K., 2012. The quantification and application of handheld energy-dispersive x-ray fluorescence (ED-XRF) in mudrock chemostratigraphy and geochemistry. Chemical Geology 324-325, 122-131.

Săndulescu, M., 1988. Cenozoic tectonic history of the Carpathians. In: Royden, L.H., Horvath, F. (Eds.), The Pannonian Basin: a study of basin evolution. AAPG Memoir 45, 17-25.

Săndulescu, M., Dumitrescu, I., 1970. Tectonic map of Romania. Institute of Geology and Geophysics. Geological Atlas 1:1,000,000. Romania.

Săndulescu, M., Micu, M., 1989. Oligocene paleogeography of the East Carpathians. In: Ghergari, L. et al. (Eds.), The Oligocene from the Transylvanian Basin. Cluj-Napoca, 79-86.

Schieber, J., 1999. Microbial mats in terrigenous clastics: The challenge of identification in the rock record. Palaios 14, 3-12.

Schieber, J., 2007. Microbial mats on muddy substrates – examples of possible sedimentary features and underlying processes. In: Schieber, J., Bose, P., Eriksson, P.G., Banerjee, S., Sarkar, S., Altermann, W., Cătuneanu, O. (Eds.), Atlas of microbial mat features preserved within the clastic rock record. Elsevier, Amsterdam, pp. 117-134.

Schieber, J., 2011. Reverse engineering mother Nature – Shale sedimentology from an experimental perspective. Sedimentary Geology 238, 1-22.

Schieber, J., 2013. SEM Observations on Ion-milled samples of Devonian Black Shales from Indiana and New York: The petrographic context of multiple pore types. AAPG Memoir 102, 153-172.

Schieber, J., 2016. Mud-redistribution in epicontinental basins – Exploring likely processes. Marine and Petroleum Geology 71, 119-133.

Schieber, J., Southard, J.B., 2009. Bedload transport of mud by floccule ripples – Direct observation of ripple migration processes and their Implications. Geology 37, 483-486.

Schieber, J., Yawar, Z., 2009. A new twist on mud deposition - Mud ripples in experiment and rock record. The Sedimentary Record 7/2, 4-8.

Schieber, J., Southard, J.B., Thaisen, K.G., 2007a. Accretion of mudstone beds from migrating floccule ripples. Science 318, December 14, 2007, 1760-1763.

Schieber, J., Sur, S., Banerjee, S., 2007b. Benthic Microbial Mats in Black Shale Units from the Vindhyan Supergroup, Middle Proterozoic of India: The Challenges of Recognizing the Genuine Article. In: Schieber, J., Bose, P., Eriksson, P.G., Banerjee, S., Sarkar, S., Altermann, W., Cătuneanu, O. (Eds.), Atlas of microbial mat features preserved within the clastic rock record. Elsevier, Amsterdam, pp. 189-197.

Schieber, J., Southard, J.B., Schimmelmann, A., 2010. Lenticular shale fabrics resulting from intermittent erosion of muddy sediments – comparing observations from flume experiments to the rock record. Journal of Sedimentary Research 80, 119-128.

Schieber, J., Southard, J.B., Kissling, P., Rossman, B., Ginsburg, R., 2013. Experimental deposition of carbonate mud from moving suspensions: importance of flocculation and implications for modern and ancient carbonate mud deposition. Journal of Sedimentary Research 83, 1025-1031.

Schieber, J., Lazar, R., Bohacs, K., Klimentidis, B., Ottmann, J., Dumitrescu, M., 2016. An SEM Study of Porosity in the Eagle Ford Shale of Texas - Pore Types and Porosity Distribution in a Depositional and Sequence Stratigraphic Context. AAPG Memoir 110, 153-172.

Schimmelmann, A., Lange, C., 1996. Tales of 1001 varves: A review of Santa Barbara Basin

sediment studies. Special Publications 116, Geological Society, London, 121-141.

Stow, D.A.V., Piper, D.J.W., 1984. Deep-water fine-grained sediments: Facies models. Special Publications 15, Geological Society, London, 611-646.

Sundborg, A., 1967. Some Aspects on fluvial sediments and fluvial morphology I. General views and graphic methods. Geografiska Annaler: Series A, Physical Geography 49:2-4, 333-343.

Ștefănescu, M., 1995. Stratigraphy and structure of Cretaceous and Paleogene flysch deposits between Prahova and Ialomita Valleys. Romanian Journal of Tectonics and Regional Geology 77, 3-49.

Talling, P.J., 2013. Hybrid submarine flows comprising turbidity current and cohesive debris flow: Deposits, theoretical and experimental analyses, and generalized models. Geosphere 9/3, June 2013, 460-488.

Terwindt, J.H.J., Breusers, H.N.C., 1972. Experiments on the origin of flaser, lenticular and sand-clay alternating bedding. Sedimentology 19, 85-98.

Triplehorn, D.M., 1966. Morphology, internal structure, and origin of glauconite pellets. Sedimentology 6, 247-266.

Yawar, Z., Schieber, J., 2017. On the origin of silt laminae in laminated shales. Sedimentary Geology 360, 22-34.